JOURNAL OF PETROLOGY | VOLUME 44 | NUMBER 9 | PAGES 1657–1679 | 2003 | DOI: 10.1093/petrology/egg052

Petrogenesis of the Largest Intraplate Volcanic Field on the Arabian Plate (Jordan): a Mixed Lithosphere–Asthenosphere Source Activated by Lithospheric Extension

JULIA E. SHAW[1,2]*, JOEL A. BAKER[1], MARTIN A. MENZIES[2], MATTHEW F. THIRLWALL[2] AND KHALIL M. IBRAHIM[3]

[1]DANISH LITHOSPHERE CENTRE, ØSTER VOLDGADE 10, COPENHAGEN, 1350 K, DENMARK

[2]DEPARTMENT OF GEOLOGY, ROYAL HOLLOWAY UNIVERSITY OF LONDON, EGHAM TW20 0EX, UK

[3]DEPARTMENT OF EARTH AND ENVIRONMENTAL SCIENCES, HASHEMITE UNIVERSITY OF JORDAN, ZARQA, JORDAN

RECEIVED JULY 1, 2002; ACCEPTED MARCH 12, 2003

Miocene to Recent volcanism in northwestern Arabia produced the largest intraplate volcanic field on the Arabian plate (Harrat Ash Shaam, Jordan). The chemically and isotopically diverse volcanic field comprises mafic alkali basalts and basanites. The magmas underwent limited fractional crystallization of ol ± cpx ± plag and rare samples have assimilated up to 20% of Late Proterozoic crust en route to the surface. However, there are subtle Sr–Nd–Pb isotopic variations ($^{87}Sr/^{86}Sr$ = 0·70305–0·70377, $^{143}Nd/^{144}Nd$ = 0·51297–0·51285, $^{206}Pb/^{204}Pb$ = 18·8–19·2), which exhibit marked correlations with major elements, incompatible trace element ratios and abundances in relatively primitive basalts (MgO >8·5 wt %), and cannot be explained by fractional crystallization and crustal contamination alone. Instead, the data require polybaric melting of heterogeneous sources. Semi-quantitative melt modelling suggests that this heterogeneity is the result of small degree melts (2–5%) from spinel- and garnet-facies mantle, inferred to be shallow Arabian lithosphere, that mixed with smaller degree melts (<1%) from a predominantly deep garnet-bearing asthenospheric(?) source with ocean island basalt characteristics. The latter may be a ubiquitous part of the asthenosphere but is preferentially tapped at small degrees of partial melting. Volcanism in Jordan appears to be the result of melting lithospheric mantle in response to lithospheric extension. With time, thinning of the lithosphere allowed progressively deeper mantle (asthenosphere?) to be activated and melts from this to mix with the shallower lithospheric mantle melts. Although Jordanian intraplate volcanism is isotopically similar to examples of Late Cenozoic volcanism throughout the Arabian peninsula (Israel, Saudi Arabia), subtle chemical and isotopic differences between Yemen and Jordan intraplate volcanism suggest that the Afar plume has not been channelled northwestwards beneath the Arabian plate and played no role in producing the northern Saudi Arabian and Jordan intraplate volcanic fields.

KEY WORDS: *asthenosphere; intraplate volcanism; Jordan; lithospheric mantle; Sr–Nd–Pb isotopes*

INTRODUCTION

The rift systems comprising the Afro-Arabian triple junction, the Red Sea and Dead Sea, as well as the continental volcanic fields that encompass this area, have been studied intensively in recent years (e.g. Freund *et al.*, 1968; Bohannon *et al.*, 1989; Menzies *et al.*, 1992; Schilling *et al.*, 1992). Oligocene flood volcanism at the Afro-Arabian triple junction in Yemen, Ethiopia, Eritrea and Djibouti was associated with continental extension and possibly the presence of a mantle plume (Chazot & Bertrand, 1993; Deniel

*Corresponding author. Telephone: ++45 3814 2665. Fax: ++45 3311 0878. E-mail: jes@dlc.ku.dk

et al., 1994; Baker *et al*., 1996; Stewart & Rogers, 1996; Pik *et al*., 1999). However, magma genesis and the geodynamic implications of the numerous intraplate volcanic fields on the Arabian plate are less clear (Camp & Roobol, 1992). In the last 15 Myr, widespread intraplate volcanism has occurred along the western margin of the Arabian peninsula (i.e. Jordan, Syria, Israel, Yemen and Saudi Arabia). This intraplate volcanism post-dates the break-up of Africa and Arabia, opening of the Red Sea, and Oligocene flood volcanism in Yemen and Ethiopia (e.g. Camp & Roobol, 1992; Baker *et al*., 1997). Although areally extensive, the Late Cenozoic intraplate volcanism is volumetrically insignificant compared with Oligocene flood volcanism in Yemen and Ethiopia (12 000 km^3 vs 350 000 km^3), which may reflect lower mantle temperatures and/or less lithospheric extension than the environment responsible for the large-volume flood volcanic province (White & McKenzie, 1989).

The Afar plume has been linked with Oligocene flood volcanism in Yemen and Ethiopia and also contributed to Pliocene–Recent intraplate volcanism in Yemen (Baker *et al*., 1996, 1997; Pik *et al*., 1999). Baker *et al*. (1997, 1998) suggested that the Yemen late-stage intraplate fields were produced by small amounts of lithospheric extension, which resulted in melting of shallow mantle that was previously metasomatized and hydrated by the Afar plume. However, magma genesis and the geodynamic implications of volcanism in northwestern Arabia farther from the influence of the Afar plume are not so clear cut. A normal mantle potential temperature of 1280°C requires a stretching factor (initial/final lithosphere thickness) of 2–5 for partial melting of dry mantle to occur (McKenzie & Bickle, 1988). This prompted Camp & Roobol (1992) to suggest that, given the small stretching factor, anomalously hot mantle is required to produce alkaline volcanism in Saudi Arabia. They hypothesized that a lobe of hot asthenosphere, believed to have originated in the Afar region, may have been channelled NW along pre-existing lithospheric flexures (e.g. Ebinger & Sleep, 1998) or that a separate mantle plume existed beneath Saudi Arabia. In contrast, Altherr *et al*. (1990) and Stein & Hofmann (1992) suggested that older shallow mantle sources produced the Saudi Arabian and Israeli alkali basalts. Stein & Hofmann (1992) speculated that an old (>200 Ma) 'fossilized' plume head had been stored in the sub-continental lithosphere and that volcanism was periodically triggered by thinning or rifting of the lithosphere.

This study focuses on the largest intraplate volcanic field on the Arabian plate (Harrat Ash Shaam). Using elemental and isotopic data, we address the following aspects of the petrogenesis: (1) the extent to which crustal processes have affected these magmas; (2) the nature of the mantle sources and the possibility that the Afar plume has been channelled northwards beneath the Arabian plate; (3) temporal and spatial relationships within the intraplate volcanic field; (4) the relationship between magma genesis of Harrat Ash Shaam and evolution of the larger Red Sea area.

GEOLOGICAL SETTING

Jordan is located at the northern end of the Red Sea where the Dead Sea plate boundary marks the transition from fully fledged oceanic rifting (i.e. central Red Sea) to trans-tensional faulting in a continental setting (Lyberis, 1988). Juvenile Pan-African basement that crops out in SW Jordan has been dated at 630–540 Ma (Ibrahim & McCourt, 1995). This basement is overlain by a series of continental and marine sandstones and limestones of Cambrian to Oligocene age. NW–SE-striking Mesozoic graben structures formed during the northeastward drift of the Arabian plate and are filled with <7 km of Cretaceous–Paleogene marine sediments. Closure of the Tethys Ocean resulted in Early Neogene regional uplift, east–west extensional tectonics, formation of the present-day Dead Sea plate boundary and initiation of compressional structures at right angles to the Mesozoic grabens (Guba & Mustafa, 1988).

Volcanism in Jordan occurs as sporadic small volcanic centres along the eastern side of the Dead Sea plate boundary and as an areally extensive intraplate volcanic field to the NE of the plate boundary (Fig. 1). Volcanism is clearly associated with continental rifting and inception of the Dead Sea plate boundary, but the exact relationship between magmatism and tectonics and the processes that have produced melt generation are unclear. Barberi *et al*. (1979) reported that alkaline volcanism in Jordan, similar to other Arabian intraplate volcanic fields, was erupted through two main fissure systems. Along the eastern margin of the Dead Sea rift the fissures trend east–west, and on the large basaltic plateau the fissures trend NW–SE. Volcanism probably commenced during the Miocene ($\sim$14 Ma) and has continued to the present day, producing a laterally extensive volcanic field (46 000 km^2) (K. M. Ibrahim, unpublished data, 1999), which is the largest single intraplate field on the Arabian plate. The volcanic field extends from Syria through Jordan and into Saudi Arabia and varies in thickness from 100 m to 1·5 km, reaching an altitude of 1800 m on the Syrian plateau. The volcanic field in Jordan itself covers an area of 11 400 km^2 (Guba & Mustafa, 1988) and is typically <150 m thick. The volcanic field comprises a series of subhorizontal lava flows <25 m thick, numerous scoria cones, extensional faults, and large

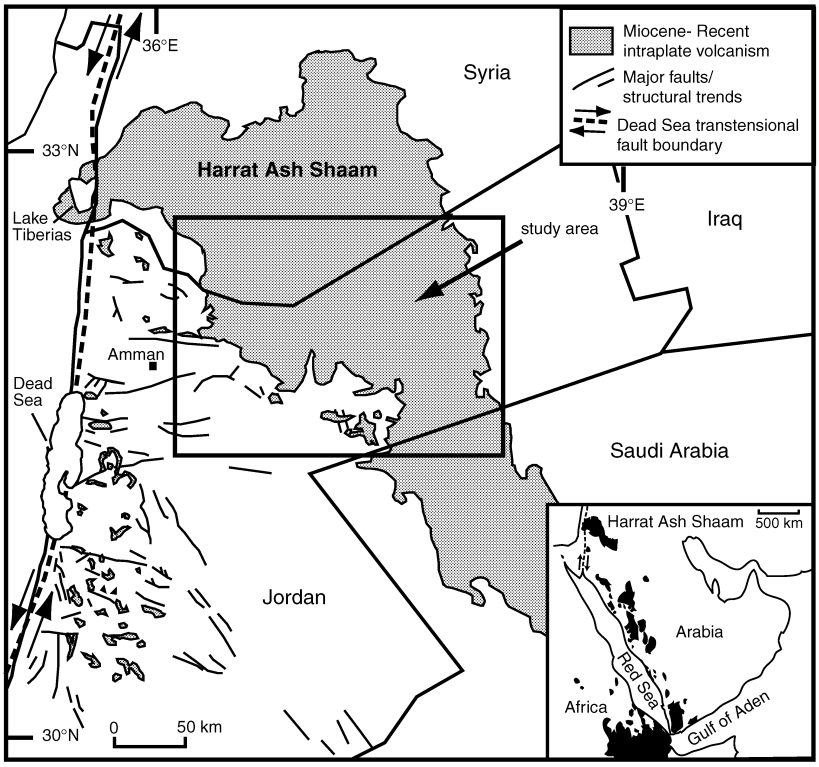

Fig. 1. Map of the Miocene–Recent intraplate volcanic field Harrat Ash Shaam, and the numerous small volcanic outcrops along the eastern margin of the Dead Sea plate boundary. Inset shows regional map of the Afro-Arabian area.

fissure eruptions that emanated from dykes <100 km in length that strike NW–SE and north–south, forming elongated ridges (K. M. Ibrahim, unpublished data, 1999). Scoria cones and fissures occur throughout the area that is covered by lava flows.

K–Ar dates from Harrat Ash Shaam (Ilani *et al.*, 2001) range from 0·05 to 40 Ma. Interestingly, only a small number of ages (5%) >14 Ma have been reported, suggesting that little volcanism occurred before 14 Ma. Volcanism appears to have been concentrated in two periods: from 0 to 8 Ma (with the majority of ages <5 Ma) and an earlier period from 8 to 14 Ma (most ages from 8 to 12 Ma). The distinct age groups will be referred to in later geochemical discussions as 'younger' and 'older'. These newly published K–Ar ages confirm earlier work by Barberi *et al.* (1979), who reported K–Ar ages of $<0{\cdot}5$ Ma to 13·7 Ma for Harrat Ash Shaam. Historical eruptions were also recorded in the 17th century (Tarawneh *et al.*, 2000). K–Ar ages from numerous intraplate volcanic fields in Saudi Arabia (Camp & Roobol, 1989, 1992; Camp *et al.*, 1991, 1992) define a period of volcanism from 0 to 12 Ma, but few ages of volcanic activity are older than 7 Ma. This followed a period of sporadic, volumetrically insignificant volcanism from 12 to 20 Ma and an older magmatic period from 20 to 32 Ma. The majority of volcanism in both Saudi Arabia and Jordan therefore appears to be younger than $\sim$12 Ma.

ANALYTICAL TECHNIQUES

Ninety-three samples were collected by the National Resources Authority of Jordan and the Geological Survey of Israel in 1999. The sampling covers the entire stratigraphic section (Ilani *et al.*, 2001) and a large proportion of the volcanic field. These samples and further sampling carried out by the authors in 2000 provide the basis for this geochemical study. Representative major and trace element and Sr–Nd–Pb isotopic data are presented in Tables 1 and 2, respectively. The full dataset is available online and may be downloaded from the *Journal of Petrology* website at http://www.petrology.oupjournals.org. Major element data were determined on fused glass discs by X-ray fluorescence spectrometry (XRF) at the Geological Institute, University of Copenhagen. Trace elements were determined on pressed powder pellets by XRF at Royal Holloway University of London (RHUL). Rare earth elements (REE) were determined on a small subset of samples at RHUL. Light rare earth elements (LREE) were determined by thermal ionization mass spectrometry (TIMS) isotope

Table 1: Representative major and trace element data and K–Ar ages for Jordan intraplate volcanic rocks (Harrat Ash Shaam)

Sample no.:	JS001	JS004	JS007	JS009	JS011	JS013	JS015	JS022	JS026	JS028	JS029	JS030	JS031	JS034	JS041	JS042
Location:	32°08·1′N	32°03·0′N	32°13·5′N	32°18·4′N	32°10·5′N	32°10·2′N	32°02·1′N	31°48·0′N	31°38·8′N	31°42·5′N	31°43·6′N	31°43·6′N	31°52·1′N	31°49·0′N	32°01·8′N	32°04·6′N
	36°57·0′E	36°51·0′E	37°13·4′E	37°29·4′E	37°07·3′E	37°06·1′E	37°58·3′E	36°44·9′E	37°15·7′E	37°19·8′E	37°21·1′E	37°21·1′E	37°26·8′E	37°31·8′E	36°30·4′E	35°34·6′E
Phenocrysts:	Ol–Pl	Ol	Ol–Pl	Ol–Px–Pl	Ol–Px	O–Pl–Px	Ol–Px	Ol	Ol–Px–Pl	Ol–Px–Pl	Ol–Px–Pl	Ol–Px–Pl	Ol	Ol	Ol	Ol–Px
wt %																
SiO_2	44·50	42·65	47·19	48·37	48·55	49·09	46·59	46·23	46·45	44·37	46·81	44·82	41·02	47·54	45·76	47·81
Al_2O_3	14·74	14·25	14·97	16·40	16·03	16·17	15·60	13·35	14·73	13·42	14·74	13·53	12·10	14·01	14·84	14·62
FeO_{total}	11·65	11·61	11·12	10·57	10·12	9·97	11·17	10·98	10·23	10·71	10·59	10·59	12·18	11·34	11·14	11·08
MgO	9·24	10·09	9·48	4·21	5·96	6·14	8·40	8·92	10·10	9·62	9·57	9·32	10·50	9·50	8·63	9·78
CaO	9·81	8·81	9·43	10·39	10·64	10·19	10·24	10·70	8·49	11·35	9·06	11·26	9·43	9·17	10·37	9·18
Na_2O	3·64	3·82	3·35	3·05	3·37	3·44	2·94	3·05	2·75	3·25	2·82	3·31	4·02	3·48	3·06	3·24
K_2O	1·529	1·069	0·974	0·815	0·990	1·024	0·796	0·891	0·580	1·043	0·544	1·006	1·137	0·993	0·937	0·881
TiO_2	2·52	3·02	2·23	2·20	2·12	2·11	2·19	2·09	1·67	2·03	1·60	2·08	2·72	2·02	2·37	1·93
MnO	0·181	0·169	0·164	0·150	0·158	0·155	0·168	0·157	0·140	0·161	0·152	0·160	0·176	0·162	0·165	0·159
P_2O_5	0·543	0·550	0·344	0·338	0·308	0·321	0·306	0·321	0·224	0·355	0·215	0·347	1·048	0·337	0·391	0·273
LOI	0·98	2·96	0·38	2·79	1·21	0·89	0·94	2·14	3·37	2·30	3·36	2·47	4·00	1·07	1·65	0·85
Total	99·33	99·00	99·63	99·28	99·44	99·50	99·33	99·84	98·73	98·61	99·45	98·89	98·34	99·61	99·30	99·79
mg-no.	0·62	0·65	0·64	0·46	0·55	0·56	0·61	0·63	0·67	0·65	0·65	0·65	0·64	0·64	0·62	0·65
ppm																
Ni	176	228	192	60	44	45	143	247	269	250	298	276	264	278	150	223
Cr	205	206	309	130	188	188	265	290	311	299	301	317	261	279	261	287
V	211	211	205	261	196	204	212	178	172	176	164	181	158	177	202	175
Sc	22·5	18·9	21·9	23·4	21·5	22·6	23·3	21·4	18·6	19·4	18·6	18·8	13·5	17·2	21·6	18·7
Cu	63·2	57·7	67·5	77·7	32·5	31·4	68·0	62·6	58·4	63·0	82·3	70·5	49·8	72·6	48·6	65·0
Zn	87·8	85·2	93·1	86·7	85·3	91·4	83·7	96·1	90·1	86·0	85·1	88·5	118·2	93·5	88·4	91·9
Cl	257	52	1123	0	0	471	129	1033	0	136	0	155	567	168	85	162
Ga	21·0	20·3	20·3	21·7	20·9	22·2	19·9	18·6	18·7	18·0	21·1	19·7	22·0	21·3	20·0	20·1
Pb	2·6	2·3	0·7	0·9	2·0	2·4	1·8	1·3	1·2	0·9	0·3	2·4	2·5	1·6	1·7	1·1
Sr	661	804	486	1071	517	490	452	659	372	567	349	626	1345	493	622	415
Rb	21·4	25·0	15·1	6·0	15·0	15·5	9·5	9·3	6·7	14·8	5·3	14·5	19·2	12·4	12·5	12·6
Ba	308	336	207	160	1029	222	200	168	125	253	160	648	348	185	230	199

Sample no.:	JS001	JS004	JS007	JS009	JS011	JS013	JS015	JS022	JS026	JS028	JS029	JS030	JS031	JS034	JS041	JS042
Location:	32°08·1′N	32°03·0′N	32°13·5′N	32°18·4′N	32°10·5′N	32°10·2′N	32°02·1′N	31°48·0′N	31°38·8′N	31°42·5′N	31°43·6′N	31°43·6′N	31°52·1′N	31°49·0′N	32°01·8′N	32°04·6′N
	36°57·0′E	36°51·0′E	37°13·4′E	37°29·4′E	37°07·3′E	37°06·1′E	37°58·3′E	36°44·9′E	37°15·7′E	37°19·8′E	37°21·1′E	37°21·1′E	37°26·8′E	37°31·8′E	36°30·4′E	35°34·6′E
Phenocrysts:	Ol–Pl	Ol	Ol–Pl	Ol–Px–Pl	Ol–Px	O–Pl–Px	Ol–Px	Ol	Ol–Px–Pl	Ol–Px–Pl	Ol–Px–Pl	Ol–Px–Pl	Ol	Ol	Ol	Ol–Px
Zr	218	230	146	153	147	146	140	135	99	136	98	133	260	151	145	124
Nb	43·8	45·6	28·5	17·8	24·2	24·3	19·6	22·5	13·6	33·5	12·5	31·6	62·5	24·5	32·5	21·7
Th	3·3	3·3	1·3	1·5	1·3	1·7	2·2	2·4	0·7	2·7	0	2·5	5·3	1·8	2·7	1·9
Y	23·1	22·0	20·9	23·1	21·0	20·5	21·0	19·4	18·9	18·4	18·6	18·9	22·8	18·0	20·4	19·8
La	25·7	26·8	17·4	15·4	16·2	16·2	12·8	12·2	8·2	17·4	7·7	16·0	47·6	14·7	18·5	14·0
Ce	60·6	61·6	43·5	34·9	40·5	38·0	36·1	38·2	24·7	39·0	22·5	35·6	103·6	35·9	45·6	35·8
Nd	29·1	31·6	21·3	20·5	21·2	20·6	19·4	20·0	13·5	19·4	12·5	19·1	49·0	18·5	23·2	18·0
K–Ar ages (Ma)	1·54	2·93	0·46	9·93	1·96	2·13	1·50	6·95	12·79	11·40	12·19	11·89	2·59	10·88	1·59	0·15
Age series	y	y	y	o	y	o	y	y	o	o	o	o	y	o	y	y

Sample no.:	JS044	JS049	JS050	JS058	JS059	JS068	JS069	JS073	JS076	JS078	JS080	JS082	JS083	JS090	JS096	JS119
Location:	32°17·1′N	32°10·7′N	32°10·7′N	32°20·2′N	32°21·8′N	32°20·6′N	32°23·1′N	31°56·8′N	32°03·1′N	32°15·6′N	32°14·2′N	32°14·2′N	32°14·2′N	31°56·3′N	31°49·0′N	32°23·2′N
	36°23·1′E	37°05·4′E	37°05·4′E	37°00·3′E	37°00·1′E	37°38·5′E	37°47·4′E	36°57·1′E	37°13·3′E	37°36·0′E	37°32·6′E	37°32·5′E	37°32·5′E	37°43·0′E	37°31·9′E	37°15·5′E
Phenocrysts:	Ol–Px	Ol–Pl	Ol	Ol–Pl	Ol–Pl	Ol	Ol–Px	Ol–Px	Ol–Px	Ol	Ol	Ol	Ol–Pl	Ol–Px	Ol–Px	Ol–Px
wt %																
SiO_2	45·44	46·17	45·82	45·00	48·50	43·31	44·03	49·61	45·88	41·58	43·46	47·03	46·16	44·26	47·32	48·26
Al_2O_3	15·01	15·30	15·65	14·25	14·67	13·57	14·04	14·94	14·17	11·51	13·85	14·38	14·38	14·60	13·91	14·61
FeO_{total}	10·78	10·45	10·69	11·77	10·81	12·69	11·67	10·45	10·55	12·92	12·60	11·06	10·62	11·77	11·33	10·76
MgO	10·03	8·43	7·83	9·07	9·82	9·48	8·70	7·11	9·32	12·21	7·76	9·46	9·06	7·71	9·83	9·60
CaO	10·49	10·84	11·21	9·88	8·78	9·93	9·70	9·61	10·80	8·31	9·46	9·64	9·92	9·12	8·99	9·04
Na_2O	3·06	3·14	3·14	3·37	3·22	4·26	2·68	3·47	3·13	5·16	4·54	3·33	2·59	4·52	3·36	3·15
K_2O	0·804	0·869	0·853	1·060	0·650	1·204	1·397	0·902	0·740	1·997	1·750	0·786	0·878	2·111	1·012	0·640
TiO_2	1·92	1·99	2·13	2·28	1·80	2·55	2·88	2·40	1·83	2·58	3·05	1·81	1·88	3·43	2·03	1·78
MnO	0·166	0·161	0·164	0·164	0·157	0·193	0·167	0·150	0·156	0·193	0·169	0·165	0·157	0·169	0·162	0·155
P_2O_5	0·304	0·341	0·311	0·370	0·224	0·719	0·609	0·265	0·268	1·062	0·643	0·350	0·344	0·692	0·342	0·211
LOI	1·10	1·61	1·66	1·96	0·52	1·03	2·71	0·43	2·29	1·18	1·84	1·30	2·99	1·23	1·17	0·80
Total	99·12	99·16	99·30	99·18	99·14	98·93	98·58	99·33	99·14	98·70	99·13	99·30	98·96	99·61	99·45	99·01
mg-no.	0·66	0·63	0·61	0·62	0·66	0·61	0·61	0·59	0·65	0·66	0·56	0·64	0·64	0·58	0·65	0·65

Table 1: continued

Sample no.:	JS044	JS049	JS050	JS058	JS059	JS068	JS069	JS073	JS076	JS078	JS080	JS082	JS083	JS090	JS096	JS119
Location:	32°17·1′N	32°10·7′N	32°10·7′N	32°20·2′N	32°21·8′N	32°20·6′N	32°23·1′N	31°56·8′N	32°03·1′N	32°15·6′N	32°14·2′N	32°14·2′N	32°14·2′N	31°56·3′N	31°49·0′N	32°23·2′N
	36°23·1′E	37°05·4′E	37°05·4′E	37°00·3′E	37°00·1′E	37°38·5′E	37°47·4′E	36°57·1′E	37°13·3′E	37°36·0′E	37°32·6′E	37°32·5′E	37°32·5′E	37°43·0′E	37°31·9′E	37°15·5′E
Phenocrysts:	Ol–Px	Ol–Pl	Ol	Ol–Pl	Ol–Pl	Ol	Ol–Px	Ol–Px	Ol–Px	Ol	Ol	Ol	Ol–Pl	Ol–Px	Ol–Px	Ol–Px
ppm																
Ni	273	144	114	235	233	203	216	117	309	429	187	221	223	151	285	236
Cr	394	287	234	255	302	216	240	240	355	446	178	288	268	181	284	308
V	207	203	213	174	185	217	210	203	180	168	190	175	179	221	177	166
Sc	24·4	23·7	25·2	18·4	22·8	19·7	18·9	22·6	18·7	11·8	16·0	18·7	19·2	16·0	17·1	20·4
Cu	82·5	54·8	57·0	63·8	62·6	86·2	62·1	50·0	89·7	39·1	57·2	70·5	66·4	55·7	72·3	54·6
Zn	83·3	86·3	78·8	96·1	94·1	116·1	104·4	92·1	89·1	150·5	118·3	92·8	91·0	96·9	95·8	92·9
Cl	70	639	61	130	443	789	72	5	225	627	800	119	0	478	571	0
Ga	18·9	20·2	19·7	21·3	18·3	23·7	24·3	21·9	20·7	23·5	25·8	20·3	19·0	25·1	20·1	18·1
Pb	1·8	1·1	0·6	1·9	1·4	1·8	2·5	2·5	2·0	4·0	1·6	0·1	2·1	3·2	0·9	0·6
Sr	464	540	459	555	351	762	1626	507	498	1240	882	675	1431	850	510	342
Rb	10·7	12·1	10·0	10·9	9·7	12·6	13·6	10·8	9·1	19·3	17·3	8·6	9·0	27·7	12·1	9·9
Ba	198	429	165	212	127	253	360	174	718	300	832	2493	147	379	228	125
Zr	134	145	140	154	116	241	233	125	125	335	276	125	130	289	151	108
Nb	24·8	27·9	20·0	28·5	14·4	53·5	38·9	21·1	17·2	117·3	72·6	37·0	22·8	54·0	25·4	12·9
Th	1·2	1·5	0·9	1·6	1·6	3·4	3·0	1·4	1·8	6·2	2·3	1·7	2·1	3·4	1·9	0·6
Y	20·2	19·6	21·1	19·5	18·9	22·7	21·5	18·3	17·4	20·0	20·8	18·5	18·5	22·4	18·2	18·3
La	13·4	18·3	13·1	16·1	8·3	33·7	26·5	10·8	10·9	52·7	30·1	15·7	15·7	31·2	15·2	9·1
Ce	31·1	41·5	32·9	40·3	27·9	79·2	63·4	29·4	27·5	117·3	72·6	37·0	38·2	74·5	36·8	30·4
Nd	15·3	21·2	19·1	19·6	16·3	37·0	33·2	18·1	15·0	52·5	35·7	19·3	19·0	36·0	18·9	16·0
K–Ar ages (Ma)	1·37	2·94	3·16	3·47	4·52	1·79	9·79	6·63	11·09	3·60	2·54	4·22	4·59	10·08	10·93	1·85
Age series	y	y	y	y	y	y	o	y	o	y	y	y	y	o	o	y

Ol, olivine; Px, pyroxene; Pl, plagioclase—these indicate the phenocryst phases present in the rock. Analytical precision/reproducibility is better than 1SD for major elements and better than 2SD for trace elements as follows: SiO_2 ±0·15 wt %; Al_2O_3 ±0·05 wt %; Fe_2O_3 ±0·1 wt %; MgO ±0·05 wt %; CaO ±0·03 wt %; Na_2O ±0·05 wt %; K_2O ±0·005 wt %; TiO_2 ±0·015 wt %; MnO ±0·003 wt %; P_2O_5 ±0·005 wt %; Ni ±1 ppm; Cr ±1·5 ppm; V ±1·5 ppm; Sc ±0·8 ppm; Cu ±1·5 ppm; Zn ±1 ppm; Cl ±20 ppm; Ga ±0·9 ppm; Pb ±0·5 ppm; Sr ±2 ppm; Rb ±0·5 ppm; Ba ±5 ppm; Zr ±1 ppm; Nb ±0·5 ppm; Th ±0·4 ppm; Y ±0·6 ppm; La ±2 ppm; Ce ±2 ppm; Nd ±1 ppm. Reproducibility increases to ±1% at high trace element concentrations. Location of samples and K–Ar ages are from Tarawneh *et al*. (2000). Age series: y, young series (0–8 Ma); o, old series (8–14 Ma). LOI, loss on ignition.

Table 2: REE isotope dilution and Nd–Sr–Pb isotopic data for Jordanian intraplate volcanic rocks (Harrat Ash Shaam)

Sample no.:	JS001	JS004	JS007	JS009	JS011	JS013	JS015	JS022	JS026	JS028	JS029	JS030	JS031	JS034	JS041	JS042
ppm																
La		28·89							9·74	19·22			51·40			
Ce		60·77							21·99	38·32			103·20			
Nd		30·65							13·27	19·50			48·68			
Sm		6·405							3·368	4·386			9·522			
Eu		2·11							1·23	1·53			3·09			
Gd		5·937							3·780	4·355			8·404			
Dy		4·406							3·407	3·575			5·064			
Er		1·916							1·781	1·686			1·776			
Yb		1·387							1·465	1·300			1·072			
Lu		0·184							0·209	0·182			0·138			
$^{87}Sr/^{86}Sr$	0·70311	0·70307	0·70359	0·70324	0·70377	0·70372	0·70330	0·70330	0·70367	0·70336		0·70350	0·70305	0·70334		0·70363
$^{143}Nd/^{144}Nd$	0·512948	0·512951	0·512877	0·512901	0·512856	0·512847	0·512911	0·512937	0·512850	0·512930		0·512930	0·512961	0·512905		0·512864
εNd	6·05	6·11	4·66	5·13	4·25	4·08	5·33	5·83	4·14	5·70		5·70	6·30	5·21		4·41
$^{206}Pb/^{204}Pb$		19·217						18·992	19·046	18·935	19·049		19·098	18·833	19·116	
$^{207}Pb/^{204}Pb$		15·588						15·597	15·606	15·587	15·610		15·574	15·589	15·634	
$^{208}Pb/^{204}Pb$		38·909						38·762	38·900	38·728	38·925		38·770	38·659	38·992	
Δ7/4		1·39						4·73	5·04	4·34	5·42		1·28	5·65	7·09	
Δ8/4		4·86						17·37	24·64	20·86	26·72		5·35	26·29	25·35	
Age series	y	y	y	o	y	y	y	y	o	o	o	o	y	o	y	y

Table 2: continued

Sample no.:	JS044	JS049	JS050	JS058	JS059	JS068	JS069	JS073	JS076	JS078	JS080	JS082	JS083	JS090	JS096	JS119
ppm																
La	14·48			17·35		36·98	29·25			55·00				31·20	16·15	10·59
Ce	30·98			37·48		75·24	62·94			113·24				70·46	34·65	23·69
Nd	16·83			20·47		36·94	32·87			53·03				35·02	18·38	14·13
Sm	3·950			4·682		7·554	7·049			10·127				7·306	4·205	3·549
Eu	1·41			1·62		2·47	2·33			3·23				2·38	1·46	1·28
Gd	4·156			4·665		6·750	6·408			8·708				6·645	3·561	3·379
Dy	3·695			3·883		4·956	4·453			4·753				4·690	3·473	3·524
Er	1·905			1·811		2·067	1·817			1·463				1·914	1·642	1·805
Yb	1·555			1·382		1·449	1·016			0·779				1·335	1·271	1·677
Lu	0·223			0·192		0·197	0·137			0·096				0·179	0·178	0·238
$^{87}Sr/^{86}Sr$	0·70331	0·70331	0·70351	0·70337	0·70357	0·70310	0·70337	0·70354	0·70373	0·70312	0·70339	0·70415	0·70331	0·70321	0·70344	0·70360
$^{143}Nd/^{144}Nd$	0·512943		0·512883	0·512892	0·512869	0·512934	0·512929	0·512895	0·512904	0·512970	0·512934	0·512899	0·512960	0·512950	0·512892	0·512887
εNd	5·95		4·78	4·95	4·51	5·79	5·68	5·21	5·19	6·48	5·77	5·09	6·28	6·07	4·95	4·86
$^{206}Pb/^{204}Pb$	19·237	18·928	19·082	19·186	19·182		19·067		19·041	18·978	19·014	18·995			18·836	19·180
$^{207}Pb/^{204}Pb$	15·605	15·621	15·641	15·647	15·654		15·606		15·618	15·563	15·586	15·588			15·583	15·643
$^{208}Pb/^{204}Pb$	38·967	38·754	38·850	38·976	39·011		38·884		38·834	38·663	38·829	38·789			38·652	38·980
Δ7/4	2·87	7·82	8·15	7·62	8·37		4·81		6·30	1·48	3·39	3·79			5·02	7·29
Δ8/4	8·25	24·30	15·29	15·31	19·30		20·50		18·64	9·16	21·41	19·70			25·23	16·44
Age series	y	y	y	y	y	y	o	y	o	y	y	y	y	o	o	y

Age series: y, young series (0–8 Ma); o, old series (8–14 Ma).

dilution analysis after chemical separation using anion exchange resin. Heavy rare earth elements (HREE) were passed through an additional set of anion exchange columns and analysed on an IsoProbe multiple-collector inductively coupled plasma mass spectrometer (MC-ICP-MS). External reproducibility for replicate LREE and HREE analyses is $<2{\cdot}5\%$ and $<3{\cdot}3\%$ (2SD), respectively. However, elemental ratios have significantly better reproducibility (Sm/Nd $\sim 0{\cdot}03\%$, Dy/Yb $\sim 0{\cdot}04\%$ 2SD, $n = 7$), reflecting the fact that weighing errors control the reproducibility of the concentration determinations. External reproducibility of BHVO-1 is generally $<1\%$ for the LREE and slightly higher (1–2%) for the HREE.

Sr–Nd–Pb isotope analyses were determined on an Axiom MC-ICP-MS at the Danish Lithosphere Centre (DLC), Copenhagen, after chemical separation using cation (Nd and Sr) and anion (Pb) exchange resins. For Sr isotope analysis, $\sim$1 g of powder was leached in 6 M HCl for $\sim$1 h at 190°C then repeatedly rinsed with MQ H_2O. Further details on analytical procedures for Nd and Sr have been described by Luais *et al.* (1997) and Waight *et al.* (2002), respectively. Waight *et al.* (2002) demonstrated that replicate analyses of standards and aqueous solutions are comparable to the reproducibilities given by TIMS analyses. Similarly, Nd isotopic analyses of BCR-1 ($0{\cdot}512634 \pm 5$) and BHVO-1 ($0{\cdot}513002 \pm 5$) by MC-ICP-MS at the DLC are within error of TIMS analyses. Internal precision (2SE) was typically better than $\pm 0{\cdot}000015$ for Sr and $\pm 0{\cdot}00001$ for Nd. External reproducibility of Sr and Nd isotope ratios is better than 0·00002 and 0·00001 (2SD), respectively. A standard was run after every four samples. Sr is reported relative to values of 0·71025 for SRM987 and Nd is reported relative to 0·512125 for an in-house AMES Nd and mixed AMES Sm–Nd standard. This Nd isotope ratio corresponds to a value of 0·51186 for La Jolla. Pb isotopic data were determined on 0·07–0·09 g of clean hand-picked rock chips. These were rinsed in MQ H_2O and leached for 1 h in hot 6 M HCl, then rinsed repeatedly in MQ H_2O before digestion and standard anion exchange separation. Pb isotopes were corrected for instrumental mass bias by internal second element normalization using Tl, and the exponential mass fractionation law. A Tl/Pb ratio of $\sim 0{\cdot}7$ and a $^{205}Tl/^{203}Tl$ ratio of 2·3889 were used, and variable Tl/Pb ratios produced no change in $^{206}Pb/^{204}Pb$ over a range of Tl/Pb ratios (0–1·5) ($\leq$100 ppm). Internal within-run precision of $^{206}Pb/^{204}Pb$, $^{207}Pb/^{204}Pb$ and $^{208}Pb/^{204}Pb$ ratios was generally better than (2SE) $\pm 0{\cdot}0021$, $\pm 0{\cdot}0017$ and $\pm 0{\cdot}0047$, respectively, although three samples had slightly worse internal precision ($\pm 0{\cdot}003$, $\pm 0{\cdot}0026$ and $\pm 0{\cdot}0055$), as a result of poor Pb yields during the chemical separation procedure. Pb isotope ratios are reported relative to $^{206}Pb/^{204}Pb = 16{\cdot}937$, $^{207}Pb/^{204}Pb = 15{\cdot}491$ and $^{208}Pb/^{204}Pb = 36{\cdot}720$ for SRM 981 with an external precision of $\pm 0{\cdot}0035$, $\pm 0{\cdot}0019$ and $\pm 0{\cdot}0055$ (2SD, $n = 8$) obtained during the course of this work. Procedural blanks were 0·5 ng, 0·05 ng and 0·075 ng for Sr, Nd and Pb, respectively, and are insignificant to this study.

PETROGRAPHY

The Jordan intraplate volcanic rocks contain 5–20 modal % phenocrysts of olivine ± plagioclase ± clinopyroxene. Olivine phenocrysts vary in size from $<0{\cdot}5$ to 3 mm and commonly have iddingsite rims or are completely altered to iddingsite. This is most common in basalts situated in the southeastern part of the intraplate field, where samples are considerably more weathered. In hand specimen, some samples are characterized by caliche lined vesicles and veins within the rock. It was not always possible to avoid this when selecting chips for crushing for chemical and isotopic analysis. Only one sample (JS049) appears to have accumulated olivine. The more primitive samples have predominantly small olivine phenocrysts (generally $<0{\cdot}5$ mm) within a cryptocrystalline groundmass. Plagioclase and clinopyroxene phenocrysts are less abundant than olivine. Evolved rocks are more coarse grained, with abundant plagioclase and clinopyroxene as well as olivine phenocrysts, and the phenocrysts are much larger (olivine phenocrysts $<\sim$3 mm) than in the more primitive samples. The groundmass is microcrystalline and consists of plag ± cpx ± ol ± Fe–Ti oxides. Phenocrysts are euhedral to subhedral in shape, and olivine and clinopyroxene are skeletal in some cases.

MAJOR AND TRACE ELEMENT CHEMISTRY

Chemical classification

The Harrat Ash Shaam volcanic rocks exhibit a wide range of silica contents (41·0–49·6 wt %) and can be classified as alkali basalts (64%), basanites (32%), hawaiites (2%) and picrobasalts (2%) using the total alkalis vs silica classification scheme (Le Bas *et al.*, 1986) (Fig. 2). The majority of samples are alkaline according to the alkaline–subalkaline classification system of MacDonald (1968), and there does not appear to be any significant change in composition in the erupted lavas from Miocene to Recent time. Compared with rock suites from the intraplate volcanic fields in Saudi Arabia and Yemen, the Jordan intraplate volcanic rocks lack more evolved compositions (Camp & Roobol, 1989; Camp *et al.*, 1991, 1992;

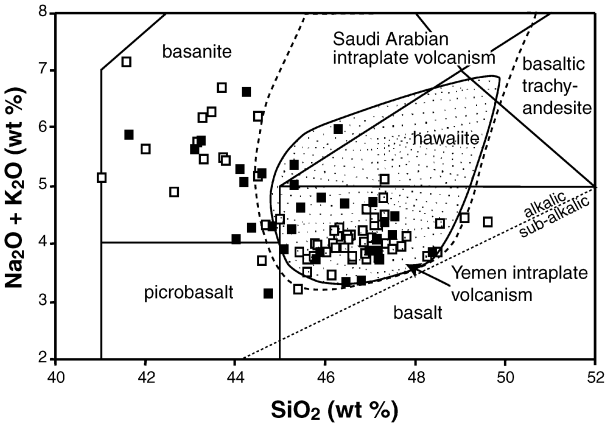

Fig. 2. Total alkalis vs silica diagram (Le Bas *et al.*, 1986) highlighting the wide range of silica saturation and the alkalic nature of the volcanic rocks. The dashed line represents the field for Saudi Arabian intraplate volcanic rocks (Altherr *et al.*, 1990) and the continuous line represents the field for Yemen intraplate volcanic rocks (Baker *et al.*, 1997). There is a lack of evolved compositions in Jordan compared with intraplate volcanic rocks from Yemen and Saudi Arabia. The alkaline–subalkaline divide is from MacDonald (1968). □, young series rocks; ■, old series rocks.

Baker *et al.*, 1997). Miocene to Recent volcanic rocks from Israel have similar compositions to the Jordanian rocks (Stein & Hofmann, 1992).

Major and trace element observations

MgO versus other major elements

MgO contents vary from 12·2 to 4·2 wt %, although most samples are restricted to 7–11 wt % (Fig. 3a–h). SiO_2, Al_2O_3 and CaO show a general increase with decreasing MgO contents. FeO (total) decreases with decreasing MgO. P_2O_5, Na_2O, K_2O and TiO_2 show little co-variation with MgO content, and there is generally large variation and scatter within the dataset. Fractionation crystallization vectors (Fig. 3a–h) show schematically that fractionation of olivine and possibly clinopyroxene has taken place, although fractionation of these phases alone can clearly not be responsible for all the major element variability. For example, at 8·5–10 wt % MgO there is significant variation in major elements, which is comparable with the entire variation displayed by the dataset as a whole. Both the younger and older series show broadly similar element concentrations and ranges.

Trace element variation

Chondrite-normalized REE patterns highlight that the Jordan intraplate volcanic rocks are strongly and variably LREE enriched relative to chondrites (La_N = 29–167) (Fig. 4a and b). All the rocks have small positive Eu anomalies (Eu/Eu^* ~1·05–1·16). REE patterns for different samples also cross, reflecting variable LREE/HREE ratios. Primitive-mantle-normalized patterns commonly peak at Nb, and are depleted in Rb relative to Ba (Fig. 4c and d). The most primitive samples have negative K and Pb anomalies, and similar patterns to some ocean-island basalts (OIB), e.g. St Helena (Weaver *et al.*, 1987; Chaffey *et al.*, 1989). Jordanian incompatible trace element ratios are similar to HIMU-type OIB; e.g. K/Nb ~144, La/Nb ~0·72, Th/La ~0·09, Ba/Nb ~5·6 for HIMU OIB (Weaver, 1991) vs K/Nb ~176, La/Nb ~0·66, Th/La ~0·11, Ba/Nb ~5·8 for Jordan. In contrast to primitive samples, some of the more evolved rocks have larger positive Ba and positive, or absent, K and Pb anomalies.

Sr–Nd–Pb ISOTOPE CHEMISTRY

Sr–Nd isotopic composition

The Jordanian intraplate volcanic rocks display the following range in Sr and Nd isotope ratios: $^{87}Sr/^{86}Sr$ = 0·70305–0·70415, $^{143}Nd/^{144}Nd$ = 0·51297–0·51285. Sr and Nd isotope ratios are strongly correlated, although there are some samples that lie above the main array. There are no distinct compositional differences between the younger and older series rocks (Fig. 5a). Cenozoic volcanic rock compositions from Israel, Saudi Arabia and Yemen are plotted for comparison in Figure 5a. Jordanian intraplate volcanic rocks extend to lower Sr isotopic values than Yemen intraplate volcanics, whereas some Saudi Arabian intraplate volcanic rocks have slightly lower $^{87}Sr/^{86}Sr$ and higher $^{143}Nd/^{144}Nd$ ratios than rocks from both Jordan and Yemen. Israeli intraplate volcanic rocks have lower $^{87}Sr/^{86}Sr$ than the majority of Jordanian rocks. Also shown in Figure 5a are possible mantle source compositions [e.g. Afar plume, Red Sea mid-ocean ridge basalt (MORB) and lithospheric mantle xenolith compositions]. Jordanian samples are isotopically more enriched (higher $^{87}Sr/^{86}Sr$ and lower $^{143}Nd/^{144}Nd$) than Red Sea MORB and overlap with compositions that are representative of the Afar plume (e.g. uncontaminated basalts from Djibouti). Lithospheric mantle xenoliths from Yemen and Saudi Arabia have a wide range of compositions and encompass nearly all the Jordanian isotopic compositions.

Pb isotopic composition

The data for Harrat Ash Shaam basalts define a restricted range of compositions in Pb isotopic space ($^{206}Pb/^{204}Pb$ = 18·83–19·24, $^{207}Pb/^{204}Pb$ = 15·56–15·65, $^{208}Pb/^{204}Pb$ = 38·65–39·01) (Fig. 6a and b). Jordanian rocks that have the most isotopically depleted Sr and Nd values lie close to the Northern

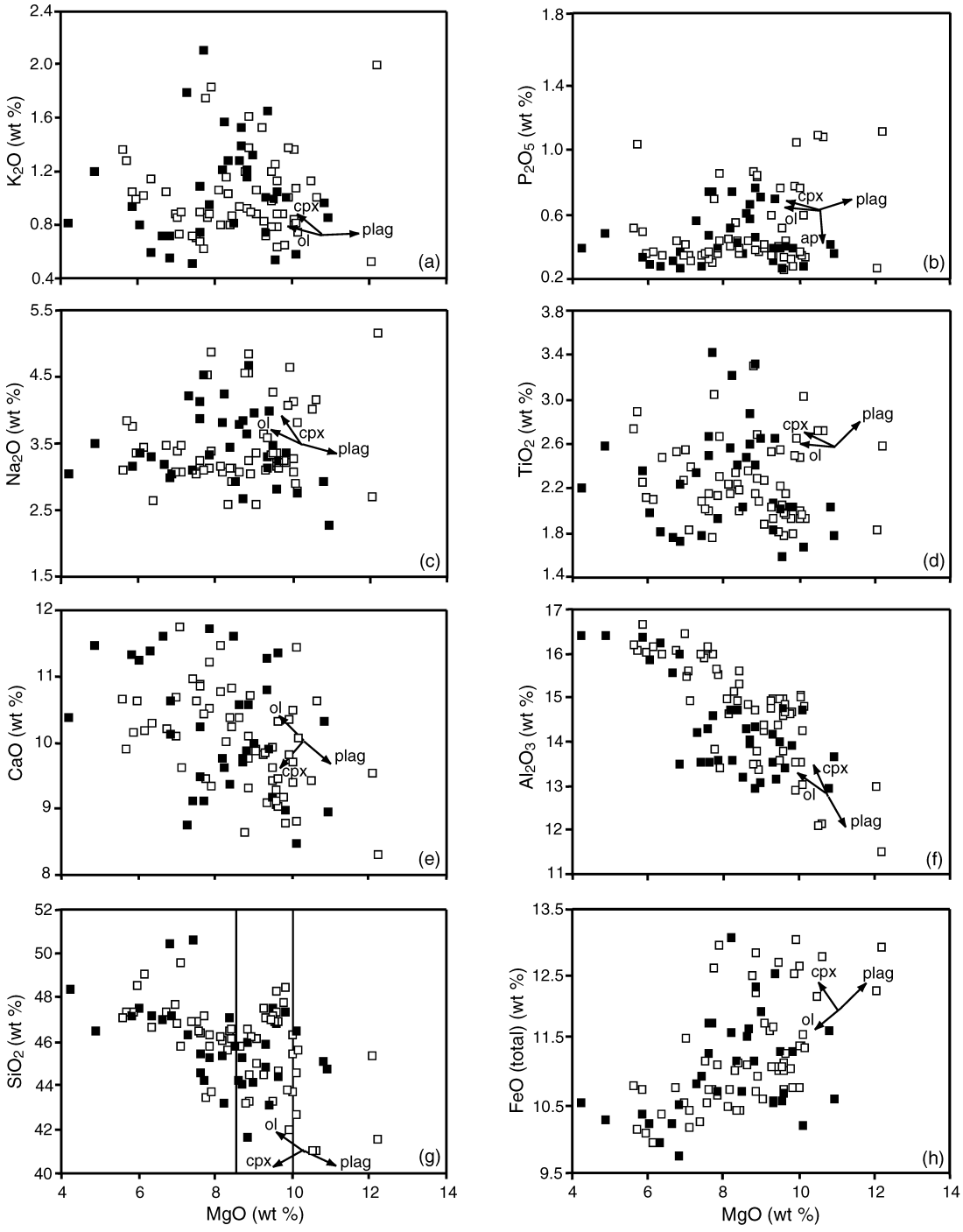

Fig. 3. (a–h) MgO vs other major element data. Diagrams are annotated with crystal fractionation vectors. The position of the vectors corresponds approximately to that estimated for a primary magma composition. Symbols are the same as in Fig. 2.

Hemisphere Reference Line (NHRL) (Hart, 1984). More enriched samples (lower $^{143}Nd/^{144}Nd$) extend to higher $^{207}Pb/^{204}Pb$ and $^{208}Pb/^{204}Pb$ compositions. In $^{206}Pb/^{204}Pb$–$^{207}Pb/^{204}Pb$–$^{208}Pb/^{204}Pb$ space Jordanian Pb isotope ratios overlap with the Afar plume, Saudi Arabian and Israel intraplate volcanic compositions, whereas the least radiogenic $^{207}Pb/^{204}Pb$ and $^{208}Pb/^{204}Pb$ compositions have similar values to the most radiogenic Red Sea MORB mantle compositions (Schilling *et al.*, 1992; Volker *et al.*, 1993). A large

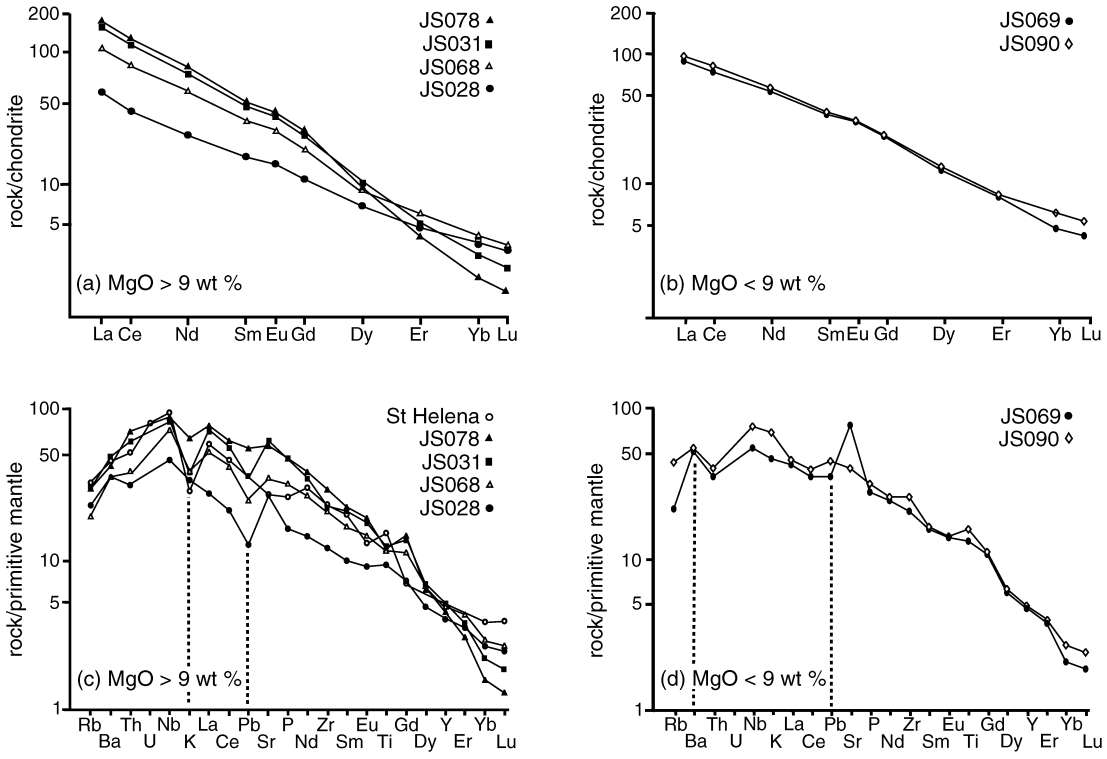

Fig. 4. (a, b) Chondrite-normalized REE diagrams, and (c, d) primitive-mantle-normalized multi-element diagrams for selected Jordan samples. (a) and (c) are primitive samples with MgO >9 wt %; (b) and (d) are evolved samples with MgO <9 wt %. Normalization values from Sun & McDonough (1989). A primitive-mantle-normalized ocean-island basalt (St Helena) has a similar pattern to the most primitive Jordan samples (data from Weaver *et al.*, 1987; Chaffey *et al.*, 1989).

proportion of the Yemen intraplate volcanic rocks are offset to lower $^{206}Pb/^{204}Pb$ (Baker *et al.*, 1997). However, a plot of $\Delta 7/4$ vs $\Delta 8/4$ (Fig. 6c) reveals subtle differences in composition between Jordanian volcanic rocks and Afar plume-related products. Afar plume-related rocks and Yemen volcanics have $\Delta 7/4$ values similar to Jordan volcanics, but the Jordan volcanics are offset to lower $\Delta 8/4$ values, and are similar to the lowest Red Sea MORB $\Delta 8/4$ ratios. The difference between Jordan intraplate volcanism and the Afar plume is not readily explained by errors resulting from mass fractionation during the analyses.

DISCUSSION

The Jordan intraplate volcanic rocks comprise alkaline basalts, basanites and hawaiites that have undergone fractionation of olivine ± plagioclase ± clinopyroxene and, although relatively mafic, are unlikely to be representative of primary magmas given their Mg numbers, and Ni and Cr contents (Table 1). There is considerable correlated variation in major and trace element abundances or ratios and isotopic ratios, but these variations are unlikely to be the product of fractional crystallization alone. There are no distinct compositional differences between the younger and older series. There are also Nd–Sr–Pb isotopic similarities between Jordan and other Arabian intraplate volcanic fields. However, the Afar plume and Yemen intraplate volcanic field appear to have higher $\Delta 8/4$ ratios, and Yemeni rocks are generally offset to lower $^{206}Pb/^{204}Pb$ ratios. We now examine the processes that may be responsible for these geochemical variations, but the focus of the discussion is on evaluating the chemical and isotopic variations in primitive samples that are difficult to explain by fractional crystallization or crustal contamination and are likely to reflect mantle processes.

Processes contributing to major and trace element and isotopic variation of Jordanian intraplate volcanism

The effects of alteration

The effects of alteration on the Jordanian intraplate volcanic rocks are difficult to assess. In thin section, the only mineral visibly affected by alteration is olivine, which is often completely or partially altered to iddingsite. However, in hand specimen caliche is present in some samples. Caliche is a common secondary growth

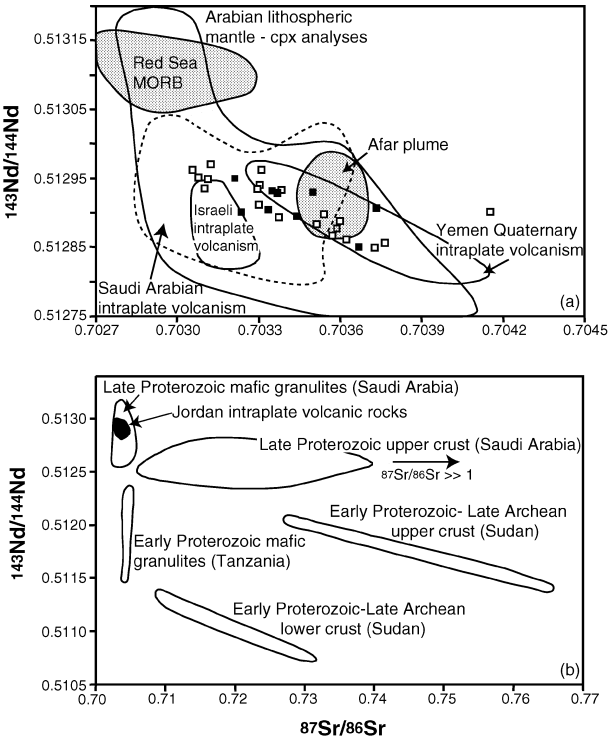

Fig. 5. Nd–Sr isotopic compositions of the Jordan volcanic rocks. Plotted for comparison are: (a) fields for Red Sea MORB (Schilling *et al*., 1992; Volker *et al*., 1993; Haase *et al*., 2000), the Afar plume (Deniel *et al*., 1994), Arabian lithospheric mantle (Blusztajn *et al*., 1995; Baker *et al*., 1998), and Yemen, Saudi Arabian and Israeli intraplate volcanism (Altherr *et al*., 1990; Stein & Hofmann, 1992; Baker *et al*., 1997), and (b) crustal compositions for Late Proterozoic upper crust from Saudi Arabia (Duyverman *et al*., 1982; Hegner & Pallister, 1989), Late Proterozoic mafic granulites from Saudi Arabia (McGuire & Stern, 1993), Early Proterozoic mafic granulites from Tanzania (Cohen *et al*., 1984), and Early Proterozoic–Late Archaean upper and lower crust from Sudan (Davidson & Wilson, 1989). $^{87}Sr/^{86}Sr \gg 1$ indicates that there are some extreme Late Proterozoic upper-crustal compositions (Duyverman *et al*., 1982) that plot off the diagram. Symbols are defined in Fig. 2.

product in arid environments, and as it occurs in cavities throughout the rock it is difficult to remove. Five samples have unusually high Ba concentrations (Ba ~647–2493 ppm) (JS011, JS030, JS076, JS080 and JS082) and high incompatible trace element ratios involving Ba (e.g. Ba/Nb, Ba/La and Ba/Th). For example, Ba concentrations and ratios in samples JS011, JS030, JS076, JS080 and JS082 are similar to, or in excess of crustal values, e.g. SW Jordan average upper-crustal values for Ba/La are ~43, and the highest Jordanian volcanic Ba/La ratio is ~158. Three of these samples (JS030, JS076 and JS082) also have high $^{87}Sr/^{86}Sr$ ratios for their $^{143}Nd/^{144}Nd$ values (Fig. 5a). Pre-digestion leaching of the samples in hot 6 M HCl should have effectively removed any radiogenic Sr introduced during alteration. However, although the measured $^{87}Sr/^{86}Sr$ ratios on leached samples are likely to reflect magmatic values, we cannot rule out the possibility of potential alteration. Nevertheless, we have included the high $^{87}Sr/^{86}Sr$ samples in the discussion. The reason for the high Ba concentrations is more difficult to assess, given that it could be a source feature or the product of secondary alteration. High Ba concentrations are unlikely to be a source feature, because there is no correlation between Ba (and trace element ratios involving Ba) and major elements, trace elements and isotopes. Secondary alteration is considered more likely, because of the presence of caliche in these Jordanian volcanic rocks. High Sr contents in some of these samples are consistent with the presence of carbonate. In the light of probable alteration effects on Ba concentrations, we have avoided using this element in the subsequent discussion.

Fractional crystallization

The phenocryst assemblages observed in the Jordan intraplate volcanic rocks suggest that variable but, in most cases, fairly limited fractionation of olivine (ol) ± plagioclase (plag) ± clinopyroxene (cpx) has occurred. Fractional crystallization vectors in Figure 3 support ol ± cpx fractionation, as do strong decreases in Ni and Cr coupled with decreasing MgO. In thin section, plagioclase appears to be an important fractionating phase, particularly in the more evolved rocks. However, plagioclase fractionation is not supported by the general lack of correlation between Sr/Nd and SiO_2–MgO, and increasing Al_2O_3 with decreasing MgO. Furthermore, at high MgO contents (8·5–10 wt %) large variations in major element (e.g. SiO_2 varies from 41·6 to 48·5 wt %) (Fig. 3) and trace element abundances (e.g. Ce varies from 22·5 to 110 ppm) make it difficult to rigorously constrain the fractionating assemblage and proportions, and highlight the need to investigate other factors responsible for major and trace element variability.

Crustal contamination?

Here we investigate the role of crustal contamination in contributing to elemental isotopic variation during magma genesis. There have been no detailed studies of the age or the composition of the crust underlying the Jordan volcanic field, but studies of the basement from SW Jordan have yielded Rb–Sr ages of 540–639 Ma (Ibrahim & McCourt, 1995). This suggests that Late Proterozoic age crust may exist beneath the Harrat Ash Shaam volcanic field. There is a large range of Nd, Sr and Pb isotopic crustal compositions from Saudi Arabia and elsewhere, which provide an indication of possible crustal contaminants (Figs 5b and 6d). However, on the basis of studies in

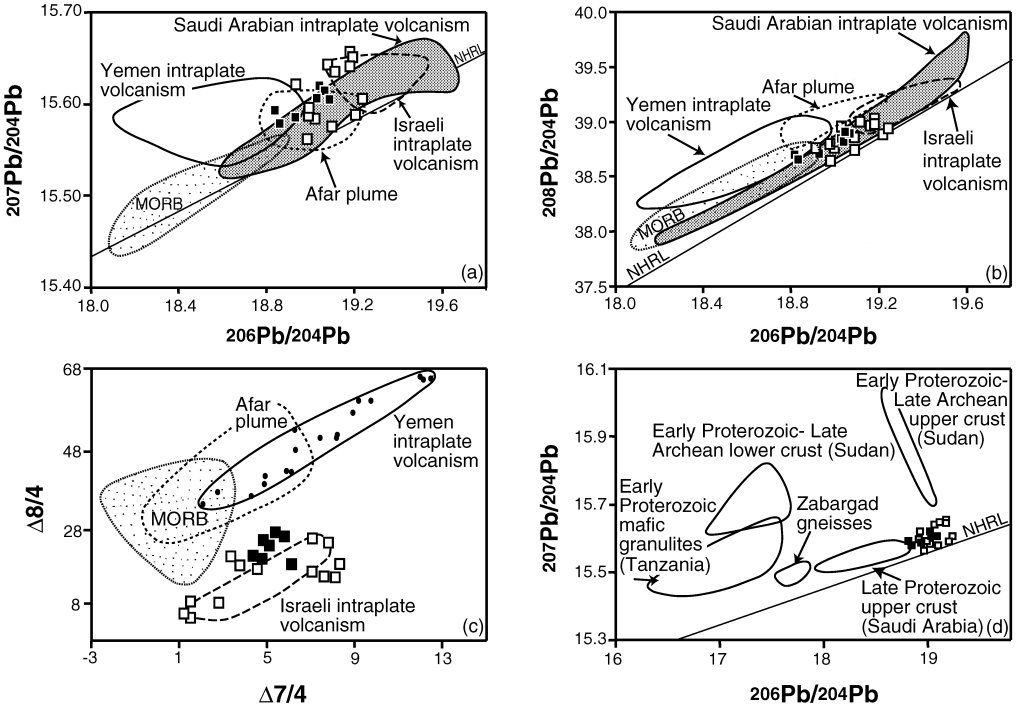

Fig. 6. (a, b) Pb isotopic compositions for Jordan intraplate volcanic rocks compared with Quaternary intraplate volcanism in Yemen (Baker *et al*., 1997), Saudi Arabia (Altherr *et al*., 1990) (excluding two samples with very high Δ7/4), and Israel (Stein & Hofmann, 1992). Also plotted for comparison are Red Sea MORB (Schilling *et al*., 1992; Volker *et al*., 1993) and the Afar plume (Deniel *et al*., 1994). Analytical uncertainty for Jordanian samples (2SD) is smaller than symbol size. (c) Δ7/4 vs Δ8/4 for Jordan volcanic rocks compared with Red Sea MORB, the Afar plume and Arabian intraplate volcanics. References are the same as for (a). (d) Pan-African Pb isotopic crustal compositions: Sudanese crust (Davidson & Wilson, 1989); Tanzanian crust (Cohen *et al*., 1984); Saudi Arabian upper crust (Hegner & Pallister, 1989); Zabargad gneisses (Brueckner *et al*., 1995). NHRL, Northern Hemisphere Reference Line (Hart, 1984). Symbols are defined in Fig. 2.

SW Jordan, it is likely that crust similar to the Arabian shield (of Late Proterozoic age and composition) is a more likely contaminant than isotopically more extreme Early Proterozoic–Late Archaean age crust found in Tanzania, Sudan and the southern Arabian shield (Yemen). On this basis, bulk mixing and assimilation–fractional crystallization (AFC) calculations were undertaken using compositions typical of this type of crust (upper crust—Duyverman *et al*., 1982; Hegner & Pallister, 1989; lower crust—McGuire & Stern, 1993). Bulk mixing and AFC trajectories in Nd–Sr isotopic space are illustrated in Figure 7a and b. The starting composition of the uncontaminated magma and the composition of the crustal contaminants are listed in Table 3. These calculations reveal the following.

(1) Up to 20% bulk assimilation of a Late Proterozoic upper-crustal component (curves 1 and 2) can account for Nd–Sr variation in the 'upper array' (Fig. 7a), which is defined by three samples (JS030, JS076 and JS082) that are offset from the main Nd–Sr isotopic array to higher $^{87}Sr/^{86}Sr$ values. Modelling using AFC curves (DePaolo, 1981) (Fig. 7b) and the appropriate crustal contaminants do not differ markedly from simple bulk mixing curves in terms of the amount of crustal contaminant required to produce the observed data array. However, although bulk mixing and AFC modelling support crustal contamination of Jordanian intraplate volcanic rocks, we cannot rule out the possibility of secondary alteration having affected samples JS030, JS076 and JS082.

(2) Assimilation of a Late Proterozoic lower-crustal component (3) can also reproduce the variation in the upper array but requires unrealistic amounts of contamination to reproduce the highest $^{87}Sr/^{86}Sr$ ratios ($\gg 50\%$) (Fig. 7a), given the similarity of lower-crustal $^{87}Sr/^{86}Sr$ ratios to contaminated Jordanian rocks. Likewise, a mixture between the two end-member bulk mixing lower-crustal curves (3 and 4) could reproduce the steeper Sr–Nd isotopic array but also requires assimilation of $\gg 50\%$ crust. These features suggest that the lower Nd–Sr isotopic array is unlikely to be the result of significant amounts of assimilation of the locally available continental crust.

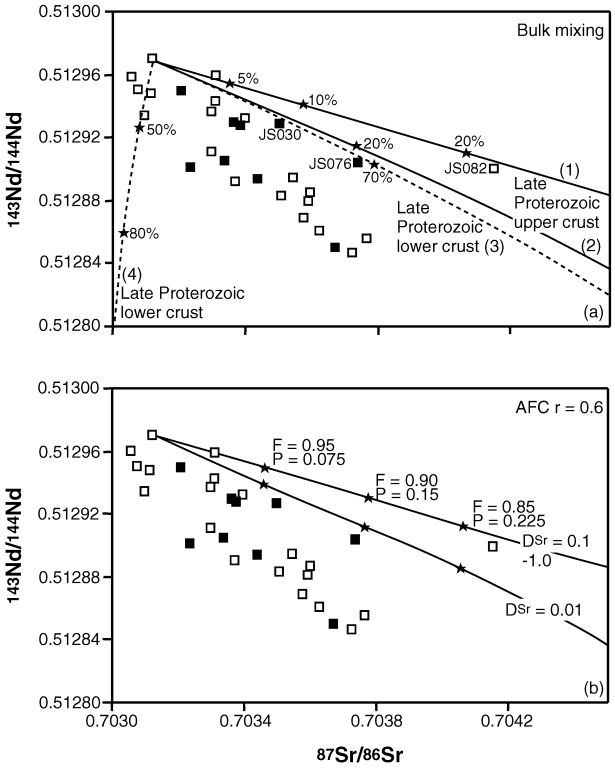

Fig. 7. (a) Bulk mixing curves illustrating the possible effects of crustal contamination on the Jordanian volcanic rocks. Continuous lines represent Late Proterozoic upper crust; dashed lines represent Late Proterozoic lower crust. (b) Assimilation–fractional crystallization calculations (DePaolo, 1981) illustrating the effects of crustal contamination. The uncontaminated basalt has the same composition as in (a); the composition of the crustal contaminant is the same as curve (1). The rate of assimilation to fractional crystallization was assumed to be 0·6. *F*, fraction of melt remaining; P, crust/magma ratio (Aitcheson & Forrest, 1994). Model parameters are given in Table 3. Symbols are as for Fig. 2.

(3) Archaean–Proterozoic silicic lower- and upper-crustal compositions from Sudan (Davidson & Wilson, 1989) have more extreme $^{87}Sr/^{86}Sr$ ($\leq$0·76) and $^{143}Nd/^{144}Nd$ ($\geq$0·51) ratios that could produce the Sr–Nd isotopic variations of the steeper array at more realistic amounts of contamination (not shown). However, this possibility can be excluded as: (a) there is no evidence for crust of this age underlying Jordan; (b) contamination by such an older crustal component would generate large changes in Pb isotopic ratios (Fig. 6d), which are not observed.

We therefore conclude that although contamination by Late Proterozoic crust may have contributed to some minor isotopic variation, it is not responsible for the major isotopic variations (e.g. the steep array in Nd–Sr isotopic space). It is important to note that there is no correlation between Mg number and Nd isotopic ratios, and that the complete range of $^{143}Nd/^{144}Nd$ is observed in samples with nearly identical and high Mg numbers. Instead, the data appear to require a heterogeneous mantle source. Strong correlations between isotopic data, major and trace element abundances and trace element ratios (next section) support this interpretation. For example, La concentrations decrease by a factor of more than five from SiO_2 of 40 to 50 wt % (Fig. 8c), and are accompanied by changing $^{143}Nd/^{144}Nd$ (0·51297–0·51284). The nature and magnitude of these correlations is not consistent with assimilation of upper or lower continental crust.

Reasons for major and trace element and isotopic variation outside the control of fractional crystallization and crustal contamination

We can explore the possible mantle source characteristics and the effects of varying degrees and depths of partial melting on major element data by reducing the effects of fractional crystallization and crustal contamination in a manner similar to that of Klein & Langmuir (1987) and Turner & Hawkesworth (1995). For this exercise, the sample set was truncated and samples with <8·5 and >10 wt % MgO were excluded. Large scatter within the dataset prevents the use of least-squares regression techniques to eliminate the effects of fractional crystallization. The three samples that were recognized as having potentially assimilated $\leq$20% continental crust (JS030, JS076 and JS082) were also excluded from further discussion. Samples within this data range (8·5–10 wt % MgO) have chemical variations not consistent with fractional crystallization processes. For example, measured FeO decreases systematically with increasing SiO_2 and decreasing Na_2O, indicative of decreasing melting pressure (i.e. depth) coupled with increasing degrees of melting (Fig. 8a and b). Na_2O, TiO_2 and K_2O are moderately incompatible in peridotite and are concentrated in small melt fractions; as such, their concentrations in a melt decrease as the degree of melting (SiO_2) increases (Klein & Langmuir, 1987; Falloon *et al.*, 1988). In contrast to Jordan, Yemen intraplate volcanic rocks (corrected to 8·5 wt % MgO by least-squares regression) are offset from the Jordan data to significantly lower $FeO_{(8·5)}$ at similar $SiO_{2(8·5)}$ and $Na_2O_{(8·5)}$ contents. This suggests different melting and/or source conditions in Yemen and Jordan and supports evidence that Yemen intraplate volcanism is the result of melting rather shallow mantle enriched and hydrated by the Afar plume (Baker *et al.*, 1997). Melting shallow hydrated mantle would result in lower FeO and higher SiO_2 contents than melting of a deeper source.

The Jordan data show strong correlations between major elements, trace elements and isotopes. SiO_2 and

Table 3: Compositions of the initial uncontaminated basalt and crustal contaminants used to calculate bulk mixing and AFC trajectories in Fig. 7

	Nd (ppm)	Sr (ppm)	$^{143}Nd/^{144}Nd$	$^{87}Sr/^{86}Sr$
Uncontaminated basalt starting composition (J78)	52·5	1240	0·51297	0·70312
(1) Late Proterozoic upper-crustal composition (high $^{87}Sr/^{86}Sr$ end-member)	26	450	0·5125	0·714
(2) Late Proterozoic upper-crustal composition (low $^{87}Sr/^{86}Sr$ end-member)	26	600	0·5125	0·708
(3) Late Proterozoic lower-crustal composition (high $^{87}Sr/^{86}Sr$ end-member)	10	300	0·51275	0·705
(3) Late Proterozoic lower-crustal composition (low $^{87}Sr/^{86}Sr$ end-member)	10	610	0·51275	0·703

Late Proterozoic upper-crustal compositions—values from Duyverman *et al*. (1982) and Hegner & Pallister (1989). Late Proterozoic lower-crustal compositions—values from McGuire & Stern (1993).

FeO exhibit good correlations with $^{143}Nd/^{144}Nd$, $^{87}Sr/^{86}Sr$ and $^{207}Pb/^{204}Pb$ ratios, Δ7/4, incompatible element abundances such as La, and incompatible trace element ratios such as K/Nb and Rb/Nb (Fig. 8c–e). $^{143}Nd/^{144}Nd$ also correlates with $^{207}Pb/^{204}Pb$ and Δ7/4 (Fig. 8f). These major element, trace element and isotopic correlations cannot be accounted for by crustal contamination and fractional crystallization processes, and suggest contributions from a heterogeneous mantle source consisting of at least one depleted and one enriched component. The depleted component has high $^{143}Nd/^{144}Nd$, and low $^{87}Sr/^{86}Sr$, Δ7/4 and Δ8/4 ratios, with variable $^{206}Pb/^{204}Pb$. Pb isotope compositions lie close to the NHRL (Fig. 6a and b). Although there are similarities with the Afar plume and Yemen intraplate volcanic rocks, Jordanian depleted samples have lower $^{208}Pb/^{204}Pb$ and Δ8/4 and encompass higher $^{143}Nd/^{144}Nd$ and lower $^{87}Sr/^{86}Sr$ compositions. None the less, incompatible trace element ratios and primitive-mantle-normalized multi-element patterns are comparable with HIMU OIB (St Helena) (Fig. 4c), and the samples are silica undersaturated (41·5–44·5 wt % SiO_2) with high MgO contents (9·5–12 wt %). Therefore, we suggest that the depleted component is more enriched than Red Sea MORB and subtly distinct from the Afar plume. For example, Figs 5a and 6c show the offset to lower $^{87}Sr/^{86}Sr$ and lower Δ8/4 than the Afar plume. Lower Δ8/4 might be explained by a long-term Th-depleted source more similar to MORB than a Th-enriched reservoir such as the continental lithosphere (Williams *et al.*, 1992).

The enriched component has low $^{143}Nd/^{144}Nd$ and high Δ7/4, Δ8/4 and $^{87}Sr/^{86}Sr$, with variable $^{206}Pb/^{204}Pb$. High Δ7/4 and low $^{143}Nd/^{144}Nd$ are coupled with higher incompatible trace element ratios than the depleted component and incompatible trace element ratios are similar to enriched OIB, e.g. EMI (Gough): K/Nb ~432 (Weaver, 1991); Jordan: K/Nb ~408.

Although it is likely that the major element, trace element and isotopic correlations reflect a chemically and isotopically heterogeneous mantle source, the large variations in major and trace element abundances must also reflect the effects of partial melting processes. For example, a negative correlation between Sm/Nd and $^{143}Nd/^{144}Nd$ (Fig. 9a) places unusual constraints on the mantle source and melting processes in the petrogenesis of the Jordanian intraplate volcanic rocks. High $^{143}Nd/^{144}Nd$ ratios suggest a long-term depleted (high Sm/Nd) source. However, the most isotopically depleted Jordanian samples (e.g. JS078: $^{143}Nd/^{144}Nd$ ~0·512970; $^{87}Sr/^{86}Sr$ ~0·703120; $^{207}Pb/^{204}Pb$ ~15·563) have the lowest Sm/Nd ratios. Low Sm/Nd ratios from a time-integrated high Sm/Nd source are likely to be the product of very low degrees of partial melting in the presence of garnet (as Nd is more incompatible than Sm). This is supported by a negative correlation between Sm/Nd and Dy/Yb and between Sm/Nd and La/Yb (Fig. 9b). Assuming a single starting composition, La/Yb or La/Y ratios reflect the degree of partial melting (La/Yb decreases with increasing degrees of melting), whereas changes in Dy/Yb ratios can be interpreted to reflect the presence of garnet in the source, as HREE are preferentially retained over the middle REE (MREE) during melting if garnet is present. These REE ratios also correlate with major elements, such as FeO and SiO_2, and with $^{143}Nd/^{144}Nd$ and Δ7/4 (Fig. 9c). Thus, mixing of small

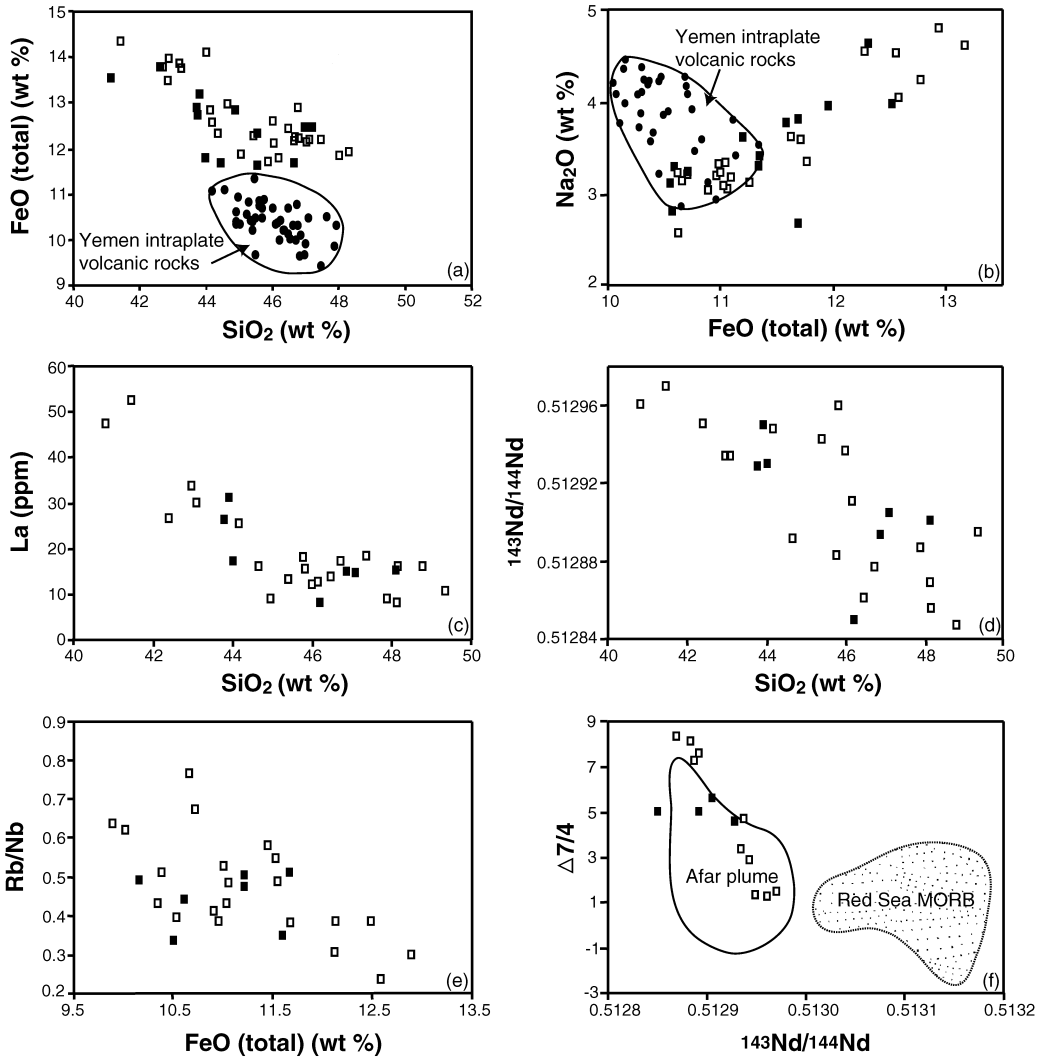

Fig. 8. (a) SiO_2 vs FeO (total); (b) FeO (total) vs Na_2O. Only Jordanian rocks with 8·5–10 wt % MgO are plotted, along with Yemen intraplate volcanic data (Baker *et al.*, 1997) (regressed to 8·5 wt % MgO using least-squares linear regression). (c–e) La (ppm) and $^{143}Nd/^{144}Nd$ ratios show a negative correlation with SiO_2, as does FeO vs Rb/Nb. (f) Red Sea MORB isotopic compositions are more depleted than Jordanian intraplate volcanics and the Afar plume. Data sources are the same as in Fig. 5a. Symbols are defined in Fig. 2.

volume melts from a deep garnet-bearing depleted mantle source with larger volume melts from an enriched shallower source can produce the isotopic–elemental co-variations observed in the Jordan intraplate volcanic rocks and provides the simplest explanation for the unusual Sm/Nd–$^{143}Nd/^{144}Nd$ correlations. Chen & Frey (1983) reported similar correlations in Hawaiian basalts and also explained this by mixing melts from an enriched mantle composition with low-degree partial melts from a MORB source.

We note that the older and younger series are not isotopically distinct in $^{143}Nd/^{144}Nd$–$^{87}Sr/^{86}Sr$ space, nor are there significant differences in major elements or trace element ratios. However, there does appear to be some temporal control on melting sources. Figure 10d shows a systematic change in $La/Y_{(N)}$ ratios with time, whereby the oldest rocks have low and restricted $La/Y_{(N)}$ ratios, and the youngest rocks have a much larger range of $La/Y_{(N)}$ values. Given that La/Y ratios reflect the degree and depth of partial melting, we suggest that the oldest volcanism in Jordan was produced by larger degrees of melting [low $La/Y_{(N)}$ ratios] of a shallow source and, with time, younger volcanism also incorporated smaller degree melts from a progressively deeper source [high $La/Y_{(N)}$ ratios].

Establishing the partial melting processes of the heterogeneous mantle source

Having established the nature of the mantle sources, and that partial melting was probably an important

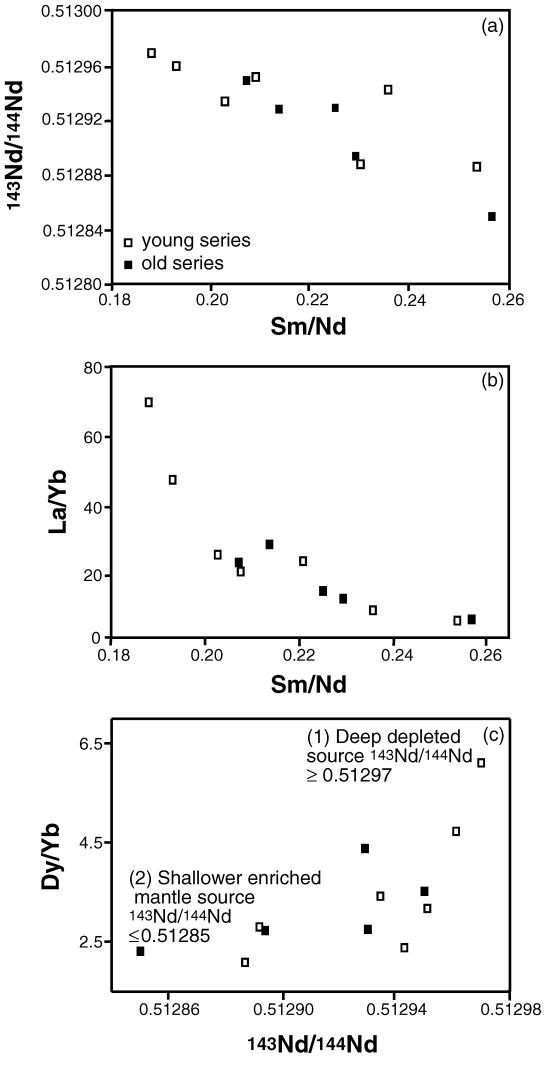

Fig. 9. (a) Sm/Nd vs $^{143}Nd/^{144}Nd$; (b) Sm/Nd vs La/Yb; (c) $^{143}Nd/^{144}Nd$ vs Dy/Yb. Negative correlations between Sm/Nd and $^{143}Nd/^{144}Nd$, and Sm/Nd and La/Yb, as well as a positive correlation between Dy/Yb and $^{143}Nd/^{144}Nd$, suggest mixing of melts from isotopically distinct mantle sources.

control on activating these sources, it is now possible to place some constraints on the conditions of partial melting. Rare earth element ratios are useful for constraining the extent and depth of partial melting along with the mineralogy and chemistry of the source. This is because the solid:melt partitioning of REE is different for garnet- and spinel-facies peridotite. Partial melting of either a garnet or spinel peridotite will preferentially enrich the LREE in the melt and produce La/Yb variations with variable degrees of melting, although the La/Yb variations will be much larger if melting garnet-facies rather than spinel-facies peridotite. Likewise, the degree of enrichment of MREE to HREE depends on whether garnet exists as a residual phase during melting, as HREE are preferentially retained by garnet during melting (high D_{Yb} ~4·0–15) relative to MREE [e.g. using distribution coefficients from McKenzie & O'Nions (1991) and Van Westrenen *et al.* (2001)]. This produces large changes in MREE/HREE ratios in melts formed by partial melting of garnet-facies peridotite, and there are large differences between source and melt ratios. In contrast, melting of a spinel peridotite will produce little change in MREE/HREE ratios with melt fraction, and their melt and source ratios are similar. Correlations between LREE/HREE (e.g. La/Yb) and MREE/HREE (e.g. Dy/Yb) will be linear when two melts of different REE composition are mixed, as the same element forms the denominator of both ratios.

Figure 10a presents $Dy/Yb_{(N)}$ vs $La/Yb_{(N)}$ data for the Jordan intraplate volcanic field, along with trajectories for non-modal fractional melts of garnet and spinel peridotite sources. Source concentrations use primitive mantle values from Taylor & McLennan (1985), which is only a crude starting approximation of the likely source concentrations. A depleted MORB mantle source (not shown) does not have La/Yb ratios high enough to reproduce Jordanian La/Yb values, even at the smallest degrees of melting in the presence of garnet. Primitive-mantle-normalized diagrams and Nd isotopic data ($\varepsilon Nd < 6{\cdot}5$) also imply a source more enriched than depleted MORB mantle. We can deduce the following points from Fig. 10a–d.

(1) Variable degrees of melting of two spinel-bearing sources cannot produce the observed variation in $Dy/Yb_{(N)}$ and $La/Yb_{(N)}$, as spinel peridotite partial melts do not have sufficient co-variation of Dy/Yb with La/Yb to produce the Jordanian data array, nor do they have sufficiently high Dy/Yb to reproduce the high Dy/Yb values of many samples (Fig. 10a).

(2) Variable degrees of melting of two garnet peridotites cannot account for the observed $La/Yb_{(N)}$–$Dy/Yb_{(N)}$ variation, as the lowest $Dy/Yb_{(N)}$ ratios of the dataset require unrealistically large degrees of melting of garnet-facies mantle (>25%). Moreover, melting of garnet-facies mantle alone would produce no co-variation between La/Yb and Yb (Fig. 10b), as Yb is retained by garnet in the source.

(3) The Jordanian rocks show small but significant co-variation between La/Yb and Yb, which suggests melting also involved a spinel-bearing source. The $La/Yb_{(N)}$–$Dy/Yb_{(N)}$ linear array (Fig. 10c) is therefore consistent with mixing melts from spinel and garnet peridotite sources.

(4) Melting of a primitive mantle source can reproduce the $La/Yb_{(N)}$ ratio of the most LREE-enriched Jordanian sample (e.g. JS078). We can use this sample

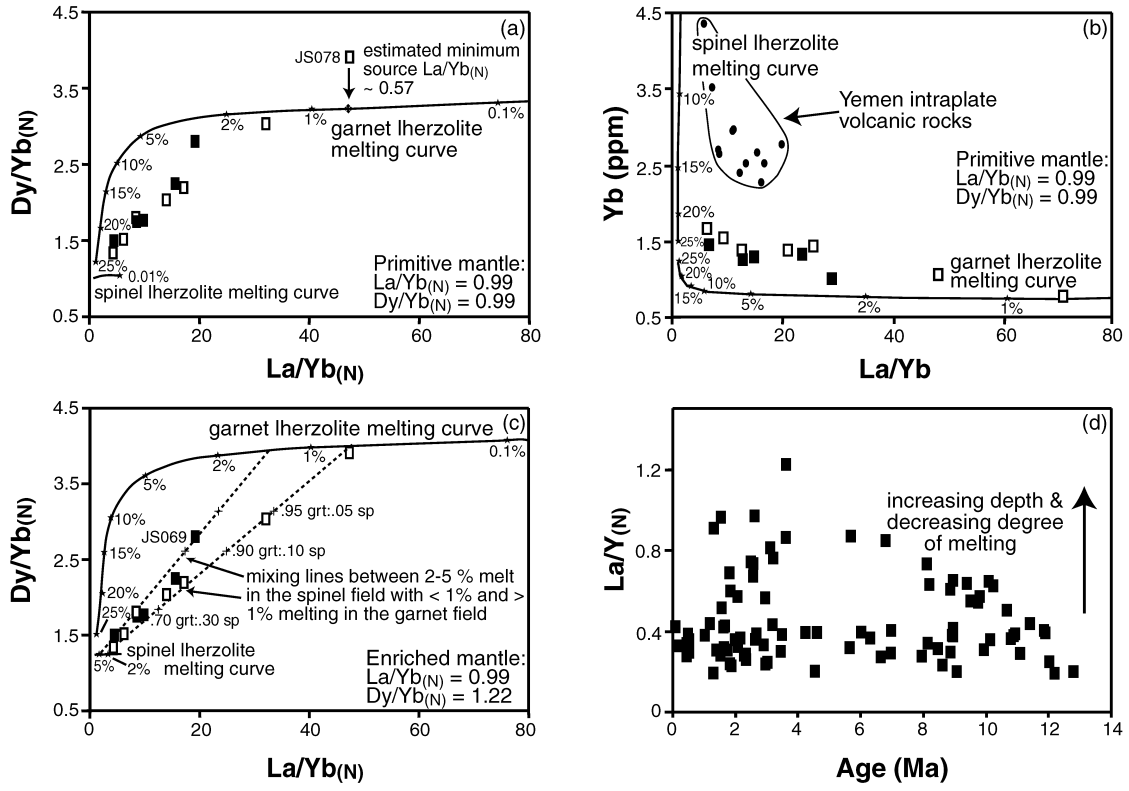

Fig. 10. (a–c) Calculated partial melting curves assuming non-modal fractional melting of garnet and spinel lherzolite sources (garnet lherzolite: 0·598 ol, 0·211 opx, 0·076 cpx, 0·115 grt that melts in the proportions 0·05 ol, 0·2 opx, 0·3 cpx, 0·45 grt; spinel lherzolite: 0·578 ol, 0·27 opx, 0·119 cpx, 0·033 sp that melts in the proportions 0·1 ol, 0·27 opx, 0·5 cpx, 0·13 sp; Thirlwall *et al.*, 1994). The composition of the primitive mantle is from Taylor & McLennan (1985). Modelling used the distribution coefficients from the compilation of McKenzie & O'Nions (1991). Stars annotated on the melting curves represent the following degrees of melting: 0·1, 1, 2, 5, 10, 15, 20 and 25%. Dashed lines represent mixing lines of partial melts from spinel- and garnet-facies mantle. (d) La/Y vs age (Ma). Yemen intraplate volcanic data from Baker *et al.* (1997). Symbols are the same as in Fig. 2.

to place some constraints on the deeper mantle source. A minimum $La/Yb_{(N)}$ ratio of the source can be determined by extrapolating the sample (JS078) downward to intersect the garnet melting curve (Fig. 10a). Although this value is dependent on source composition [as increasing the source $La/Yb_{(N)}$ ratio stretches the melting curve parallel to the $La/Yb_{(N)}$ axis], we estimate a minimum value of $La/Yb_{(N)}$ ~0·57 using a primitive mantle source. As this sample is unlikely to represent 0·01% melting, a source with $La/Yb_{(N)} > 0{\cdot}57$ is probable. This is more enriched than a depleted MORB source, which has $La/Yb_{(N)}$ ~0·4. Changing the garnet/clinopyroxene (grt/cpx) ratio also extends the melting curve parallel to the $La/Yb_{(N)}$ axis. However, published mineral proportions of garnet peridotites (Johnson, 1998; Putirka, 1999) do not differ significantly from our model value of grt/cpx = 1·5. Our only upper constraint on the $La/Yb_{(N)}$ ratio is from Nd isotopes of the depleted source end-member ($^{143}Nd/^{144}Nd$ ~0·51297), which suggest long-term LREE depletion relative to a chondritic mantle source [$\sim La/Yb_{(N)} < 1$], but not as extreme as depleted MORB mantle.

(5) A primitive mantle source cannot produce the highest $Dy/Yb_{(N)}$ ratio of the sample set. This requires a minimum source Dy/Yb_N ratio of 1·22 (Fig. 10c). This is unlikely to be coupled with corresponding La enrichment given that a long-term LREE-depleted source is likely. Increasing grt/cpx ratios also raises $Dy/Yb_{(N)}$ ratios, but in this case maximizing the grt/cpx ratio using the given mineral proportions cannot raise the garnet melting curve to intersect the sample (JS078). Furthermore, modelling partial melting of garnet pyroxenites or eclogites that have much greater modal garnet cannot increase the Dy/Yb ratio, as grt/cpx ratios are often less than that of a garnet peridotite. A garnet distribution coefficient ratio (D_{Dy}/D_{Yb}) $\leq 0{\cdot}2$ will also produce the necessary $Dy/Yb_{(N)}$ ratios, although garnet distribution coefficients are still poorly constrained. For example, garnet distribution coefficients from Johnson (1998) and Van Westrenen *et al.* (2001) are up to four times greater than those in the

compilation reported by McKenzie & O'Nions (1991), and have D_{Dy}/D_{Yb} ratios of 0·33 and 0·39, respectively. This results in translation of the melting curve to lower Dy/Yb values.

In summary, melting appears to be polybaric, occurring over an extended depth range from garnet-bearing to garnet-absent mantle (i.e. spinel-facies mantle). For example, some samples appear to be derived totally from garnet-facies mantle whereas others are dominated (~75%) by melts from the spinel field (Fig. 10c). Combining this information with temporal controls on volcanism, we conclude that earliest volcanism appears to involve predominantly shallower and larger degree melts (2–5%), from a spinel-bearing (and probably also garnet-bearing) isotopically enriched source. With time, volcanism incorporated a greater proportion of deeper, smaller degree melts (<1%) from an isotopically depleted garnet-bearing source. An older series sample (JS069) offset from the main trend to lower $La/Yb_{(N)}$ can be accounted for by slightly larger degrees of melting of the garnet-bearing source (Fig. 10c).

Jordanian intraplate volcanism within the regional tectonic setting

Normal Arabian lithosphere is 100–120 km thick (Mooney *et al.*, 1985). The upper lithosphere (or mechanical boundary layer) is presumed to comprise crust and spinel-facies (<80 km) and garnet-facies (>80 km) lithospheric mantle. The lower lithosphere will comprise garnet-facies mantle, which overlies and is influenced by the asthenosphere (1300°C). Consistent with the presence of 100–120 km thick lithosphere, surface heat flow measurements over western Arabia are lower than the world average (400–500°C at 40–50 km depth) (Gettings, 1981; Gettings *et al.*, 1986). However, this is in contrast to temperatures calculated from mantle xenolith data, which suggest mantle temperatures of 900–1100°C at similar depths (Camp *et al.*, 1992). The lack of agreement between surface and mantle temperatures was suggested as evidence for the presence of upwelling asthenosphere beneath western Arabia (McGuire & Bohannon, 1989). To what extent this mantle is normal temperature, or hotter than normal, may be influenced by the influx of hotter mantle originating as far south as Afar that is directed northward by 'topography' on the base of the lithosphere, as proposed by Ebinger & Sleep (1998).

In the context of the petrogenesis of the Jordanian intraplate volcanic rocks, the temporal and spatial evolution of the volcanic field can be summarized as follows. Volcanic rocks were initially derived from shallow, isotopically slightly enriched, spinel- and garnet-facies mantle by ~2–5% melting. Given the thickness of the lithosphere (>100 km), the depth of melting and the distinct isotopic characteristics, we propose that the enriched source is located within the lithospheric mantle. With time, these melts mixed in varying proportions with melts predominantly derived from deeper, isotopically depleted, garnet-facies mantle generated by very small degrees of melting (<1%). Considering lithospheric thicknesses, we propose that the depleted source (>80 km) is likely to be located within the asthenosphere or the lowermost part of the lithospheric mantle.

This scenario is consistent with a model of progressive lithospheric rifting and thinning with time. The extended depth range over which melting occurs (from 100% garnet-facies derived melts to 100% spinel-facies derived melts) suggests a melting regime controlled by lithospheric extension. This is also supported by xenolith data, from which the asthenosphere–lithosphere boundary is estimated to be at a depth of ~75 km (McGuire & Bohannon, 1989) compared with >100 km before thinning and rifting. The thermal boundary layer (i.e. the lower lithospheric mantle or the asthenosphere) is melted in response to thermal erosion of the lithosphere by upwelling asthenosphere driven by lithospheric extension. This allows small degree garnet-facies melts to mix with larger degree melts from spinel-facies (and garnet-facies) mantle as extension and volcanism proceeds.

Jordanian intraplate volcanism is isotopically similar in many respects to examples of Late Cenozoic volcanism throughout the Arabian peninsula (Israel, Saudi Arabia). Volcanism in Israel and Saudi Arabia is thought to have been derived from a shallow mantle source, perhaps enriched by an old plume head that periodically produced volcanism in response to lithospheric thinning (Altherr *et al.*, 1990; Stein & Hofmann, 1992). It is likely that both Israel and Saudi Arabian volcanism are tapping similar mantle sources to the Jordanian volcanism. In contrast to Jordan, Yemen intraplate volcanism displays the influence of the Afar plume with shallower levels of melting of a hydrated (e.g. lower FeO and Dy/Yb) and a subtly distinct isotopic source (e.g. higher $\Delta 8/4$ than the Jordanian samples) (Baker *et al.*, 1997). Given these chemical and isotopic contrasts, we conclude that the Afar plume has not been channelled northwards beneath the Arabian plate.

CONCLUSIONS

Miocene to Recent volcanism in northwestern Arabia produced the largest intraplate volcanic field on the Arabian plate (Harrat Ash Shaam, Jordan). The following conclusions can be gleaned from this study.

(1) The chemically and isotopically diverse volcanic field comprises mafic alkali basalts and basanites. Most magmas have undergone only limited fractional crystallization of ol ± cpx ± plag, and rare samples have assimilated up to 20% of Late Proterozoic crust en route to the surface. Jordanian intraplate volcanic rocks lack the evolved compositions of intraplate volcanic rocks from Saudi Arabia and Yemen, as the extensional environment permitted ascent of more mafic magmas in Jordan, which did not undergo protracted fractionation.

(2) Large coupled variations in major elements, trace elements and Sr–Nd–Pb isotopes (e.g. a negative correlation between Sm/Nd and $^{143}Nd/^{144}Nd$) cannot be explained by fractional crystallization and crustal contamination alone and require polybaric melting of heterogeneous mantle sources. This involves 2–5% melting of a shallow spinel- and garnet-facies mantle source that represents Arabian lithosphere. Melts from this mix in variable proportions with smaller degree melts ($<1\%$) from a deep garnet-bearing lithospheric or asthenospheric source. This source might be a minor ambient component of the asthenosphere preferentially tapped at small degrees of melting.

(3) Volcanism in Jordan is consistent with a model in which polybaric melting of distinct sources occurred in response to lithospheric extension. Extension first triggered partial melting of shallow lithospheric mantle. As extension progressed and asthenosphere upwelled, these melts mixed with smaller degree melts from deep (asthenospheric?) mantle.

(4) Jordanian intraplate volcanism is isotopically similar in many respects to examples of Late Cenozoic volcanism throughout the Arabian peninsula (Israel, Saudi Arabia). In contrast to Jordan, Yemen intraplate volcanism displays the influence of the Afar plume with shallower levels of melting of a hydrated and a subtly distinct isotopic source. We conclude that the Afar plume has not been channelled northwards beneath the Arabian plate and probably played no role in many of the northern Saudi Arabian, Israeli and Jordan intraplate volcanic fields.

ACKNOWLEDGEMENTS

We are grateful to the National Resources Authority of Jordan and the Geological Survey of Israel. Thoughtful and constructive reviews from David Peate, Nick Arndt, Karsten Haase and the editor Pamela Kempton improved the quality of the manuscript. The Danish Lithosphere Centre (DLC) and Royal Holloway University of London are thanked for the joint funding of a Ph.D. studentship that made this project possible. The DLC is supported by the Danish National Research Foundation. This paper is part of the doctoral research of J.E.S.

SUPPLEMENTARY DATA

For supplementary data, please refer to *Journal of Petrology* online.

REFERENCES

Aitcheson, S. J. & Forrest, A. H. (1994). Quantification of crustal contamination in open magmatic systems. *Journal of Petrology* **35**, 461–488.

Altherr, R., Henjes-Kunst, F. & Baumann, A. (1990). Asthenosphere versus lithosphere as possible sources for basaltic magmas erupted during formation of the Red Sea: constraints from Sr, Pb and Nd isotopes. *Earth and Planetary Science Letters* **96**, 269–286.

Baker, J. A., Thirlwall, M. F. & Menzies, M. A. (1996). Sr–Nd–Pb and trace element evidence for crustal contamination of plume-derived flood basalts: Oligocene flood volcanism in western Yemen. *Geochimica et Cosmochimica Acta* **60**, 2559–2581.

Baker, J. A., Menzies, M. A., Thirlwall, M. F. & Macpherson, C. G. (1997). Petrogenesis of Quaternary intraplate volcanism, Sana'a, Yemen: implications for plume–lithosphere interaction and polybaric melt hybridization. *Journal of Petrology* **38**, 1359–1390.

Baker, J., Chazot, G., Menzies, M. & Thirlwall, M. (1998). Metasomatism of the shallow mantle beneath Yemen by the Afar plume—implications for mantle plumes, flood volcanism, and intraplate volcanism. *Geology* **26**, 431–434.

Barberi, F., Capaldi, G., Gasperini, P., Marinelli, G., Santacroce, R., Scandone, R., Treuil, M. & Varet, J. (1979). Recent basaltic volcanism of Jordan and its implications on the geodynamic evolution of the Dead Sea Shear Zone. *Atti die Convegni Lincei* **47**, 667–683.

Blusztajn, J., Hart, S. R., Shimizu, N. & McGuire, A. V. (1995). Trace-element and isotopic characteristics of spinel peridotite xenoliths from Saudi Arabia. *Chemical Geology* **123**, 53–65.

Bohannon, R. G., Naeser, C. W., Schmidt, D. L. & Zimmermann, R. A. (1989). The timing of uplift, volcanism, and rifting peripheral to the Red Sea: a case for passive rifting? *Journal of Geophysical Research* **94**, 1683–1701.

Brueckner, H. K., Elhaddad, M. A., Hamelin, B., Hemming, S., Kröner, A., Reisberg, L. & Seyler, M. (1995). A Pan-African origin and uplift for the gneisses and peridotites of Zabargad Island, Red Sea: a Nd, Sr, Pb, and Os isotope study. *Journal of Geophysical Research* **100**, 22283–22297.

Camp, V. E. & Roobol, M. J. (1989). The Arabian continental alkali basalt province: Part I. Evolution of Harrat Rahat, Kingdom of Saudi Arabia. *Geological Society of America Bulletin* **101**, 71–95.

Camp, V. E. & Roobol, M. J. (1992). Upwelling asthenosphere beneath western Arabia and its regional implications. *Journal of Geophysical Research* **97**, 15255–15271.

Camp, V. E., Roobol, M. J. & Hooper, P. R. (1991). The Arabian continental alkali basalt province: Part II. Evolution of Harrats Khaybar, Ithnayn, and Kura, Kingdom of Saudi Arabia. *Geological Society of America Bulletin* **103**, 363–391.

Camp, V. E., Roobol, M. J. & Hooper, P. R. (1992). The Arabian continental alkali basalt province: Part III. Evolution of Harrat

Kishb, Kingdom of Saudi Arabia. *Geological Society of America Bulletin* **104**, 379–396.

Chaffey, D. J., Cliff, R. A. & Wilson, B. M. (1989). Characterisation of the St Helena magma source. In: Saunders, A. D. & Norry, M. J. (eds) *Magmatism in the Ocean Basins. Geological Society, London, Special Publications* **42**, 257–276.

Chazot, G. & Bertrand, H. (1993). Mantle sources and magma–continental crust interactions during early Red Sea–Gulf of Aden rifting in Southern Yemen: elemental and Sr, Nd, Pb isotope evidence. *Journal of Geophysical Research* **98**, 1819–1835.

Chen, C.-Y. & Frey, F. A. (1983). Origin of Hawaiian tholeiite and alkalic basalt. *Nature* **302**, 785–789.

Cohen, R. S., O'Nions, R. K. & Dawson, J. B. (1984). Isotope geochemistry of xenoliths from East Africa: implications for development of mantle reservoirs and their interaction. *Earth and Planetary Science Letters* **68**, 209–220.

Davidson, J. P. & Wilson, I. R. (1989). Evolution of an alkali basalt–trachyte suite from Jebel Marra volcano, Sudan, through assimilation and fractional crystallisation. *Earth and Planetary Science Letters* **95**, 141–160.

Deniel, C., Vidal, P., Coulon, C., Vellutini, P.-J. & Piquet, P. (1994). Temporal evolution of mantle sources during continental rifting: the volcanism of Djibouti (Afar). *Journal of Geophysical Research* **99**, 2853–2869.

DePaolo, D. J. (1981). Trace element and isotopic effects of combined wallrock assimilation and fractional crystallisation. *Earth and Planetary Science Letters* **53**, 189–202.

Duyverman, H. J., Harris, N. B. W. & Hawkesworth, C. J. (1982). Crustal accretion in the Pan-African: Nd and Sr isotope evidence from the Arabian Shield. *Earth and Planetary Science Letters* **59**, 315–326.

Ebinger, C. J. & Sleep, N. H. (1998). Cenozoic magmatism throughout east Africa resulting from impact of a single plume. *Nature* **395**, 788–791.

Falloon, T. J., Green, D. H., Hatton, C. J. & Harris, K. I. (1988). Anhydrous partial melting of a fertile and depleted peridotite from 2 to 30 kb and application to basalt petrogenesis. *Journal of Petrology* **29**, 1257–1282.

Freund, R., Zak, I. & Garfunkel, Z. (1968). Age and rate of the sinistral movement along the Dead Sea rift. *Nature* **220**, 253–255.

Gettings, M. E. (1981). A heat flow profile across the Arabian Shield and Red Sea. *EOS Transactions, American Geophysical Union* **62**, 407.

Gettings, M. E., Blank, H. R., Mooney, W. D. & Healey, J. H. (1986). Crustal structure of southwestern Saudi Arabia. *Journal of Geophysical Research* **91**, 6491–6512.

Guba, I. & Mustafa, H. (1988). Structural control of young basaltic fissure eruptions in the plateau basalt area of the Arabian plate, Northeastern Jordan. *Journal of Volcanology and Geothermal Research* **35**, 319–334.

Haase, K. M., Mühe, R. & Stoffers, P. (2000). Magmatism during extension of the lithosphere: geochemical constraints from lavas of the Shaban Deep, northern Red Sea. *Chemical Geology* **166**, 225–239.

Hart, S. R. (1984). A large-scale isotope anomaly in the Southern Hemisphere mantle. *Nature* **309**, 753–757.

Hegner, E. & Pallister, J. S. (1989). Pb, Sr and Nd isotopic characteristics of Tertiary Red Sea rift volcanics from the central Saudi Arabian coastal plain. *Journal of Geophysical Research* **94**, 7749–7755.

Ibrahim, K. M. & McCourt, W. J. (1995). Neoproterozoic granitic magmatism and tectonic evolution of the northern Arabian Shield: evidence from southwest Jordan. *Journal of African Earth Sciences* **20**, 103–118.

Ilani, S., Harlavan, Y., Tarawneh, K., Rabba, I., Weinberger, R., Ibrahim, K., Peltz, S. & Steinitz, G. (2001). New K–Ar ages of basalts from the Harrat Ash Shaam volcanic field in Jordan: implications for the span and duration of the upper mantle upwelling beneath the western Arabian plate. *Geology* **29**, 171–174.

Johnson, K. T. M. (1998). Experimental determination of partition coefficients for rare earth and high-field-strength elements between clinopyroxene, garnet, and basaltic melt at high pressures. *Contributions to Mineralogy and Petrology* **133**, 60–68.

Klein, E. M. & Langmuir, C. H. (1987). Global correlations of ocean ridge basalt chemistry with axial depth and crustal thickness. *Journal of Geophysical Research* **92**, 8089–8115.

Le Bas, M. J., Le Maitre, R. W., Streckeisen, A. & Zanettin, B. (1986). A chemical classification of volcanic rocks based on the total alkali–silica diagram. *Journal of Petrology* **27**, 745–750.

Luais, B., Telouk, P. & Albarède, F. (1997). Precise and accurate neodymium isotopic measurements by plasma-source mass spectrometry. *Geochimica et Cosmochimica Acta* **61**, 4847–4854.

Lyberis, N. (1988). Tectonic evolution of the Gulf of Suez and the Gulf of Aqaba. *Tectonophysics* **153**, 209–220.

MacDonald, G. A. (1968). Composition and origin of Hawaiian lavas. *Geological Society of America, Memoir* **116**, 477–522.

McGuire, A. V. & Bohannon, R. G. (1989). Timing of mantle upwelling: evidence for a passive origin for the Red Sea rift. *Journal of Geophysical Research* **94**, 1677–1682.

McGuire, A. V. & Stern, R. J. (1993). Granulite xenoliths from western Saudi Arabia: the lower crust of the late Precambrian Arabian–Nubian Shield. *Contributions to Mineralogy and Petrology* **114**, 395–408.

McKenzie, D. & Bickle, M. J. (1988). The volume and composition of melt generated by extension of the lithosphere. *Journal of Petrology* **29**, 625–679.

McKenzie, D. & O'Nions, R. K. (1991). Partial melt distributions from inversion of rare earth element concentrations. *Journal of Petrology* **32**, 1021–1091.

Menzies, M. A., Baker, J., Bosence, D., Dart, C., Davison, I., Hurford, A., Al'Kadasi, M., McClay, K., Nichols, G., Al'Subbary, A. & Yelland, A. (1992). The timing of magmatism, uplift and crustal extension: preliminary observations from Yemen. In: Storey, B. C., Alabaster, T. & Pankhurst, R. J. (eds) *Magmatism and the Causes of Continental Break-up. Geological Society, London, Special Publications* **68**, 293–304.

Mooney, W. D., Gettings, M. E., Blank, H. R. & Healy, J. W. (1985). Saudi Arabian seismic deep refraction: a travel-time interpretation of crust and upper mantle structure. *Tectonophysics* **111**, 173–246.

Pik, R., Deniel, C., Coulon, C., Yirgu, G. & Marty, B. (1999). Isotopic and trace element signatures of Ethiopian flood basalts: evidence for plume–lithosphere interactions. *Geochimica et Cosmochimica Acta* **63**, 2263–2279.

Putirka, K. (1999). Melting depths and mantle heterogeneity beneath Hawaii and the East Pacific Rise: constraints from Na/Ti and rare earth element ratios. *Journal of Geophysical Research* **104**, 2817–2829.

Schilling, J.-G., Kingsley, R. H., Hanan, B. B. & McCully, B. L. (1992). Nd–Sr–Pb isotopic variations along the Gulf of Aden: evidence for Afar mantle plume–continental lithosphere interaction. *Journal of Geophysical Research* **97**, 10927–10966.

Stein, M. & Hofmann, A. W. (1992). Fossil plume head beneath the Arabian lithosphere? *Earth and Planetary Science Letters* **114**, 193–209.

Stewart, K. & Rogers, N. (1996). Mantle plume and lithosphere contributions to basalts from southern Ethiopia. *Earth and Planetary Science Letters* **139**, 195–211.

Sun, S.-S. & McDonough, W. F. (1989). Chemical and isotopic systematics of oceanic basalts: implications for mantle composition and processes. In: Saunders, A. D. & Norry, M. J. (eds) *Magmatism in the Ocean Basins*. *Geological Society, London, Special Publications* **42**, 313–345.

Tarawneh, K., Ilani, S., Rabba, I., Harlavan, Y., Peltz, S., Ibrahim, K., Weinberger, R. & Steinitz, G. (2000). Dating of the Harrat Ash Shaam Basalts, northeast Jordan. *Jordan Natural Resources Authority and Geological Survey of Israel Report* **GSI/2/2000**, 59 pp.

Taylor, S. R. & McLennan, S. M. (1985). *The Continental Crust: its Composition and Evolution*. Oxford: Blackwell Science.

Thirlwall, M. F., Upton, B. G. J. & Jenkins, C. (1994). Interaction between continental lithosphere and the Iceland plume—Sr–Nd–Pb isotope geochemistry of Tertiary basalts, NE Greenland. *Journal of Petrology* **35**, 839–879.

Turner, S. & Hawkesworth, C. (1995). The nature of the subcontinental mantle: constraints from the major-element composition of continental flood basalts. *Chemical Geology* **120**, 295–314.

Van Westrenen, W., Wood, B. J. & Blundy, J. D. (2001). A predictive thermodynamic model of garnet–melt trace element partitioning. *Contributions to Mineralogy and Petrology* **142**, 219–234.

Volker, F., McCulloch, M. T. & Altherr, R. (1993). Submarine basalts from the Red Sea: new Pb, Sr, and Nd isotopic data. *Geophysical Research Letters* **20**, 927–930.

Waight, T., Baker, J. & Peate, D. (2002). Sr isotope ratio measurements by double-focusing MC-ICPMS: techniques, observations and pitfalls. *International Journal of Mass Spectrometry* **221**, 229–244.

Weaver, B. L. (1991). The origin of ocean island basalt end-member compositions: trace element and isotopic contraints. *Earth and Planetary Science Letters* **104**, 381–397.

Weaver, B. L., Wood, D. A., Tarney, J. & Joron, J. L. (1987). Geochemistry of ocean island basalts from the South Atlantic: Ascension, Bouvet, St Helena, Gough and Tristan da Cunha. In: Fitton, J. G. & Upton, B. G. J. (eds) *Alkaline Igneous Rocks*. *Geological Society, London, Special Publications* **30**, 253–267.

White, R. & McKenzie, D. (1989). Magmatism at rift zones: the generation of volcanic continental margins and flood basalts. *Journal of Geophysical Research* **94**, 7685–7729.

Williams, R. W., Collerson, K. D., Gill, J. B. & Deniel, C. (1992). High Th/U ratios in subcontinental lithospheric mantle: mass spectrometric measurement of Th isotopes in Gaussberg lamproites. *Earth and Planetary Science Letters* **111**, 257–268.